Spring 7-23-2015

Feasibility Study of Prestressed Natural Fiber-Reinforced Polylactic Acid (PLA) Composite Materials

Sean A. Hinchcliffe
University of Colorado at Boulder, sean.h@live.com

FEASIBILITY STUDY OF PRESTRESSED NATURAL FIBER-REINFORCED POLYLACTIC ACID (PLA) COMPOSITE MATERIALS

by

SEAN A. HINCHCLIFFE

B.S., Oregon Institute of Technology, 2013

A thesis submitted to the

Faculty of the Graduate School of the

University of Colorado in partial fulfillment

of the requirement for the degree of

Master of Science

Department of Civil, Environmental, and Architectural Engineering

2015

This thesis entitled:

Feasibility Study of Prestressed Natural Fiber-Reinforced

Polylactic Acid (PLA) Composite Materials

written by Sean A. Hinchcliffe

has been approved for the Department of Civil, Environmental, and Architectural Engineering

_____

DR. WIL SRUBAR

_____

DR. PETROS SIDERIS

_____

DR. YUNPING XI

Date: _____

The final copy of this thesis has been examined by the signatories, and we find that both the content and the form meet acceptable presentation standards of scholarly work in the above mentioned discipline.

ABSTRACT

Hinchcliffe, Sean A. (M.S., Department of Civil, Environmental, and Architectural Engineering)

Feasibility Study of Prestressed Natural Fiber-Reinforced Polylactic Acid (PLA) Composite Materials

Thesis directed by Assistant Professor Wil V. Srubar III

The feasibility of manufacturing high-performance, prestressed natural-fiber reinforced biopolymer composites is demonstrated in this work. The objective of this study was to illustrate that the specific mechanical properties of biopolymers, namely polylactic acid (PLA), can be enhanced by leveraging a combination of (a) additive manufacturing (3D printing) and (b) initial post-tensioning of continuous natural fiber reinforcement. In this study, both tensile and flexural PLA specimens of various cross-sectional geometries were 3D-printed with and without post-tensioning ducts. The mechanical properties of two continuous reinforcing fibers, jute and flax, were characterized prior to threading, post-tensioning to a prescribed level of stress, and anchoring using a mechanical loading frame. The effect of fiber type, matrix cross-sectional geometry, number of reinforcing strands, and degree of post-tensioning on the specific mechanical properties (e.g., strength-to-weight, stiffness-to-weight) of PLA were investigated using both tensile and flexural mechanical testing. Finite element models of a subgroup of the composite specimens were developed and the same experimental tests were simulated using the models. Additionally, analytical equations were derived for the prediction of composite tensile mechanical properties.

Experimental results confirm that 3D-printed matrices improve the specific tensile and flexural mechanical properties of PLA composites and that these properties are further improved via initial fiber prestressing. The experimental data indicate statistically significant increases (*p*-

value < 0.05) in specific strengths of 116% and 32% and specific stiffnesses of 62% and 29% in tension and flexure, respectively, compared to unreinforced PLA specimens. The results suggest that both additive manufacturing and fiber prestressing represent viable new methods for improving the mechanical performance of natural fiber-reinforced polymeric composites. Finite element model simulation results, as well as results from mechanics-based analytical equations, for mechanical behavior of the composite specimens aligned well with obtained data, thus further strengthening the validity of the experimental results. This study considered only mechanical behavior of natural fiber-reinforced biopolymeric composites; the need remains for future research in other aspects (e.g., long-term durability, economic constraints) in order to further demonstrate the viability of these novel composite materials for construction applications.

ACKNOWLEDGMENTS

I would like to thank my advisor, Dr. Wil Srubar, for his guidance and support throughout my graduate student career. I would also like to thank my other two committee members, Dr. Petros Sideris and Dr. Yunping Xi, for providing their and feedback and helpful recommendations on my work.

I would like to acknowledge Kristen Hess and the other members of the Sustainable Infrastructure Materials Laboratory (SIMLab) at the University of Colorado Boulder for their collaboration and constructive input to my research. Financial support through the CEAE Department and CEAE Bridge-Term Fellowship is also gratefully acknowledged.

CONTENTS

TABLES

FIGURES

CHAPTER 1
Introduction

1.1 Motivation and Background

As the need for infrastructure development and renewal increases worldwide, synthetic fiber-reinforced polymer (FRP) composite materials have gained attention in recent years as alternatives to more traditional infrastructure materials, primarily due to their favorable durability, mechanical, weight, and cost characteristics [1-3]. Advances in improving the performance of FRP composites have further increased their attractiveness as primary infrastructure materials and in other applications. However, environmental concerns accompany increased use of traditional FRPs. First, they contribute to the already significant amount of construction and demolition debris being deposited into landfills each year, which totaled 88 million tons in 2003 [4]. Most current commercial FRPs are comprised of petroleum-based synthetic matrices, such as epoxies and polyurethane, and synthetic fibers, such as glass, carbon, and aramid [5]. The exceptional durability characteristics of synthetic FRPs comprised of these materials that make them desirable for many applications can conversely be problematic in post-use and disposal phases, due to their resistance to degradation and the energy required to separate and recycle them [6]. Second, the production of petroleum-based FRP composite materials requires large amounts of energy and contributes to the depletion of limited natural petroleum resources [7].

Therefore, investigation into the viability of fully biobased FRP composite material alternatives (i.e., natural fibers contained within a biopolymer matrix) has been of increasing interest in recent years. Polymers and composites from renewable resources are being engineered for target applications not only in construction industries, but also in automotive and packaging

industries at historically high rates to address growing environmental concerns of a globally unsustainable dependence on petroleum-based resources and to counter the proliferation of synthetic polymers and plastics in the environment.

Many biopolymers, such as polylactic acid (PLA), as well as cellulosic natural fibers, are readily biodegradable (i.e., degrade naturally into harmless products) [8], and thus could potentially alleviate waste recalcitrance problems [9]. In addition to biodegradability, fully biobased composite materials exhibit low embodied energy, inherent renewability, and have the potential to have a closed-loop lifecycle rather than a traditional linear (i.e., production, in-service use, disposal) lifecycle [6,9]. The biopolymer matrix components of biobased FRPs are commonly produced by microbial synthesis (e.g., polyhydroxyalkanoates [PHAs], polyhydroxybutyrate-co-valerate [PHBV]) or from agricultural byproducts (e.g., PLA). A number of biopolymers have been shown to possess mechanical properties (e.g., strength and stiffness) comparable to those of synthetic polymer matrices [10,11]. The natural fiber reinforcement constituents of FRPs commonly originate from plant sources such as sisal, hemp, jute, and flax. Several of these natural fibers have been shown to exhibit competitive mechanical properties (e.g., strength and stiffness) and are lower in weight compared to traditional synthetic fiber reinforcement [12-16]. In addition to enhancing mechanical performance and reducing material cost, the use of natural fibers as reinforcement in polymeric composites has gained favor due to attributes such as biodegradability, availability, and economic viability. Natural fibers are generally cheaper to process, easier to handle, require less production energy, and originate from more locally available and renewable resources than their synthetic counterparts [2]. The combining of a biobased polymer matrix and a natural fiber reinforcement produces a FRP composite with considerable potential environmental and economic advantages.

A variety of natural alternatives to synthetic fibers (e.g., carbon, glass, aramid) and conventional petroleum-based polymers (e.g., polypropylene, polyethylene), have been evaluated for natural fiber composite (NFC) applications [17-20]. Previous work has focused primarily on the mechanical characterization of isotropic, short-fiber composites made from a variety of natural fibers (e.g., hemp, flax, jute, sisal, wood flour) [21-23]. Investigations of continuously woven natural fabrics have also been carried out on pultruded hybrid specimens (not fully biobased) of hemp and continuous glass fibers [24]. In the last decade, hemp linen and jute burlap have been used as reinforcement in fully biobased composites with resins of PLA, polyhydroxybutyrate (PHB), and their copolymers [9,25,26].

The tensile strength and elastic moduli of these composites vary widely (depending on their individual constituents), with many achieving properties similar to wood and engineered products [27,28]. A list of mechanical properties of selected natural fibers, biopolymers, and fully biobased composites is shown in **Table 1**. As mentioned, natural fibers from plants and animals (e.g., silk) exhibit excellent tensile mechanical properties (e.g., strength, stiffness), adding to other advantages such as low cost, rapid renewability, and global availability. Mechanical properties of fully biobased composites made from these polymers and natural fibers are also shown in **Table 1**. The properties of these composites are comparable to wood and engineered wood materials, like plywood (also shown). However, differences are apparent in the relative densities of these materials. For example, fully biobased composites are approximately three times the density of conventional wood products. Thus, it is evident from the data in **Table 1** that the mechanical properties of natural fibers are not fully utilized in composite form.

Table 1. Selected material properties of natural fibers, biopolymers, biobased composites, and wood products (for comparison) [9,11,27,29-32].

Material	Tensile Strength (MPa)	Tensile Modulus (GPa)	Tensile Elongation (%)	Flexural Strength (MPa)	Flexural Modulus (GPa)	Density (kg/m^3)
Natural Fiber						
Hemp (Bast) Fiber	270-900	20-90	1-4	-	-	1500
Jute (Bast) Fiber	200-800	10-35	1-2	-	-	1450
Flax (Bast) Fiber	300-1500	25-100	1-4	-	-	1400
Kenaf (Bast) Fiber	200	15-34	1-4	-	-	1400
Abaca (Leaf) Fiber	500-750	6-30	1-7	-	-	1500
Silk (*Bombyx mori*)	200-750	5-17	20	-	-	1300
Biopolymer						
PHB	40-45	3.5-4	5-8	50-60	3	1180-1260
PLA	21-60	0.4-3.5	2-6	40-60	2-4	1210-1250
PGA	60-100	6-7	1.5-20	150	7.6	1500-1700
Natural Fiber-Biopolymer Composites						
Hemp/PHB	56	5.5	2-8	65	6.5	1270-1310
Wood Flour/PLA	-	-	-	28	2.3	1200-2200
Wood Flour/PHB	20-40	3.5-5	0.5-2	40	5.9	1800-2900
Wood and Engineered Wood						
Douglas-Fir	-	-	-	75-90	13.4	480
Western Hemlock	-	-	-	70-85	11.3	450
Pine	-	-	-	40-65	8.9	400
Plywood	27	10.3	-	27	10.3	400-810
Oriented Strand Board	-	-	-	21.2	5.3	490-810
Glue-laminated wood	-	-	-	26-72	10.6	320-720

Although the advantages are promising, the disadvantages of fully biobased FRP composite materials cannot be ignored. One of the most significant drawbacks is mechanical performance — while they approach the mechanical properties of traditional synthetic FRPs, those of fully biobased FRPs still require improvement to become more competitive. Another, potentially more prohibitive disadvantage is the current high cost of producing biopolymers on a

bulk scale. The high production cost is not due to the material itself, but rather the current state of technological development of biopolymer manufacturing processes — synthetic polymer manufacturing has existed for many decades, while biopolymer manufacturing is more recent [17,33]. The cost of biopolymer production, however, is expected to decrease as technology and manufacturing processes improve.

Another disadvantage of biobased polymers is their high density, which can be unfavorable in applications where low weight and high specific properties are favored. Natural fibers have disadvantages as well, including considerable variability in quality from manufacturing and processing, long-term durability concerns due to moisture absorption and ultraviolet degradation, and poor resistance to high temperatures [34-36]. Natural fiber variability stems from a number of causes (e.g., plant source, growth conditions, inconsistent microstructure, defects, moisture content, age) and extraction and processing techniques [37,38]. In order to improve the viability and feasibility of fully biobased FRP composites, the above enumerated disadvantages and challenges must be addressed with further scientific investigation.

1.2 Potential for Prestressed Natural Fiber Composites (NFCs)

Much research has been performed on the mechanical properties of synthetic FRP composites over the course of many decades. A large portion of this research has focused on continuous-fiber-, short-fiber-, and particle-reinforced composites (bonded composites). While research on synthetic FRPs is substantial and long-standing, research on FRP composite configurations containing either a biobased reinforcing fiber or a biobased polymer matrix has only emerged in the last two decades. These partially biobased, or hybrid, FRPs are defined as either a synthetic fiber within a biopolymer matrix or a natural fiber within a synthetic polymer

matrix. The latter configuration, primarily due to the availability of synthetic polymers and natural fibers, has been studied in more depth than the former configuration [2]. Research areas on this type of natural fiber-reinforced polymer (NFRP) range from quantifying environmental impacts [39,40], to characterizing mechanical properties and comparing with commonly-used synthetic fibers [15,16,41-43].

A smaller body of research has focused on fully biobased FRP composites, which consist of natural fiber reinforcement contained within a biobased polymer matrix. Many of these studies have investigated the improvement of mechanical properties via more effective fiber-matrix interfacial bonding [13,23,33,42,44]. Other studies have investigated mechanical performance improvements by shape optimization and cellular structure utilization [6,45-47] — current research has shown that reductions in density and improvements in specific mechanical properties of biopolymers and natural fiber composites can be achieved by foaming [47-49] and engineering foam-core sandwich structures [28]. Multiscale modeling and long-term durability of biobased composites have also been investigated, but only preliminarily [50,51]. Due to their generally inferior mechanical properties, the majority of research regarding fully biobased FRPs has concentrated on improving these properties [52-54].

Virtually no research, however, has investigated utilizing the effects of prestressing/post-tensioning in natural fiber reinforcement of biopolymer FRPs as a means to improve mechanical performance. Prestressing of reinforcement, a technique used in the reinforced concrete industry that is predicated on providing improved mechanical performance through the utilization of superior compressive behavior of the composite matrix (concrete) and high tensile strength of the reinforcement (steel tendons) [55,56], is believed to be effective in the application of NFCs. Their biopolymer matrices and natural fiber reinforcement exhibit high compressive strength and high

tensile strength characteristics, respectively, as concrete and steel in prestressed concrete applications. Moreover, prestressing of reinforcement generally reduces tensile forces in the composite matrix that cause cracking and ultimate tensile failure [55] — a desirable effect for biopolymer matrices, many of which are weaker in tension and exhibit failure by brittle fracture. The effect of prestressed reinforcement on the flexural stresses of a flexural member are demonstrated below in **Figure 1**. As noted, the magnitude of the internal tensile stresses (denoted with a "T" in **Figure 1**) during flexure are reduced with the addition of prestressing forces in the reinforcement.

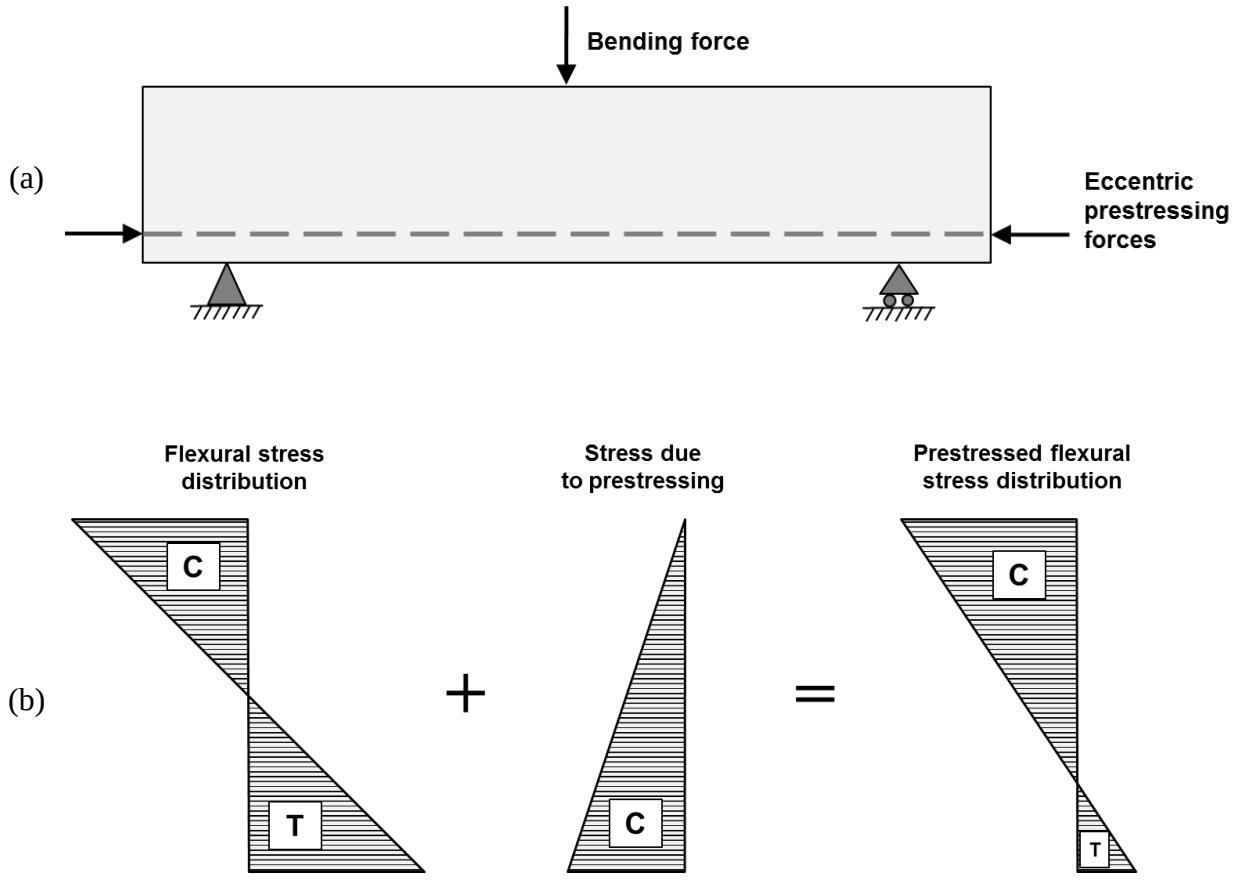

Figure 1. Schematic showing (a) an elevation view of a prestressed beam subject to bending and (b) the beam stress distributions resulting from flexure and prestressing [56].

While previous studies have investigated the effect of fiber prestressing on the mechanical behavior of *synthetic* fibers, namely glass [57], ultra-high molecular weight polyethylene [58], and nylon-kevlar [59] fiber composites, no studies have yet reported on the viability or effects of prestressing continuous natural fiber reinforcement, which has the potential to provide similar mechanical improvements as found in such studies.

The two most common methods of prestressing synthetic fiber-reinforced polymers (FRPs) involve (a) pre-tensioning fibers prior to application of epoxy-based (thermoset) matrices [60] or (b) pre-tensioning entire FRP composite laminates prior to external bonding to concretes structures [1,61]. The majority of existing literature on prestressed FRP composites concerns the latter, with primary application to the retrofit of concrete structures [1,62]. In previous ply- and laminate-level studies of synthetic FRPs, Motahhari and Cameron [57] found that the flexural modulus and strength of glass-epoxy composites increased 33% through initial fiber prestressing. The experimental data also indicated a fiber prestressing level (approximately 50% of ultimate stress) at which flexural properties reached maximum values. Similarly, other studies have shown that prestressing unidirectional glass fibers increases the flexural deflection and strength of dental resins by 60% and 30%, respectively [63]. However, no FRP studies have applied a prestressing technique frequently employed by the prestressed concrete industry, in which the prestressing tendons are not bonded with the matrix (unbonded prestressing) and are anchored in place at either end of the structural element. Analogous to an unbonded prestressed concrete structural member in this application, the polymer matrix of a prestressed FRP would act similar to the concrete, and the natural fibers similar to the prestressed steel tendons.

Given the proven success of prestressing synthetic fibers, the inherently high stiffness and strength of natural fibers, and the ability of additive manufacturing to form complex, structural geometries, there is significant potential to improve the specific mechanical properties of natural-fiber composites. However, to the author's knowledge, the viability and feasibility of prestressing natural fibers for high-performance NFCs has yet to be sufficiently proven.

1.3 Thesis Organization

The primary objective of this research was to demonstrate that the specific mechanical properties of natural-fiber biocomposites can be improved by (a) leveraging 3D printing capabilities and (b) applying a prestressing technique to the natural fiber reinforcement. This thesis is divided into five chapters, throughout which the efficacy of cross-sectional shape and post-tensioning of non-bonded natural fiber reinforcement on improving the specific mechanical properties of fully biobased FRP composite structural members is investigated.

This first chapter elucidates the main motivation, objectives, and goals of this thesis. Chapter 2 and Chapter 3 present the experimental methods and results obtained from tensile and flexural mechanical testing, respectively, of unstressed and prestressed NFC structural members. Chapter 2 provides an overview of the characterization of the tensile mechanical properties of both jute and flax reinforcing fibers and of the compressive mechanical properties of PLA, the manufacture and preparation of non-fiber-reinforced and fiber-reinforced composite tensile specimens (including prestressing fibers to prescribed levels of pretensioning), the characterization of mechanical properties of the NFCs, and comparison of mechanical properties between groups of tensile specimens. Chapter 3 is structured similarly to Chapter 2, but focuses on flexural NFC structural member experimental testing rather than tensile testing. In Chapter 4, two models are

presented. First, numerical finite element model simulations, created for the purpose of comparison with the flexural experimental tests, are presented and discussed. Second, analytical equations that predict the tensile mechanical properties of the specimens described in Chapter 2 are derived, and their results are discussed. Chapter 5 provides conclusions drawn from the research presented in previous chapters, as well as challenges and opportunities remaining to be addressed in the future. Appendices A and B contain raw force-displacement data from the tensile and flexural testing, respectively, and are organized by specimen type.

CHAPTER 2
Experimental Tensile Testing

2.1 Overview

Dogbone-shaped PLA specimens of two (2) cross-sectional geometries were manufactured for experimental tensile testing. Next, two (2) types of natural fibers were experimentally tensile tested and subsequently mechanically characterized to determine their effectiveness in the prestressing application. Compressive mechanical testing and characterization of solid PLA was then performed. Then, solid, unreinforced, and prestressed fiber-reinforced composite PLA tensile specimens were prepared. Finally, the PLA and fiber-reinforced PLA tensile specimens were experimentally tested in order to characterize mechanical properties. Results for specific (weight-normalized) mechanical properties were calculated from the experimental testing data for each specimen type and compared between groups to determine the influence of cross-sectional geometry and fiber reinforcement on mechanical properties.

2.2 Materials and Experimental Methods

2.2.1 Materials

Natural jute fibers (2.0 mm diameter) and flax fibers (0.5 mm diameter) were commercially obtained from a local hardware supply store. True white- and natural-colored polylactic acid (PLA) was supplied in spooled filament form (1.8 mm diameter) by MakerBot Industries, LLC.

2.2.2 Experimental methods

2.2.2.1 Tensile specimen manufacture and preparation

PLA tensile dogbone specimens were computer-modeled according to ASTM D638 standards and 3D-printed using a MakerBot 5th-Generation Replicator Desktop 3D printer. The extruder temperature, resolution, and print speed were set to 215 °C, 0.2 mm, and 60 mm/s, respectively. A photograph of the 3D printer used to manufacture the PLA matrices is shown in **Figure 2** below.

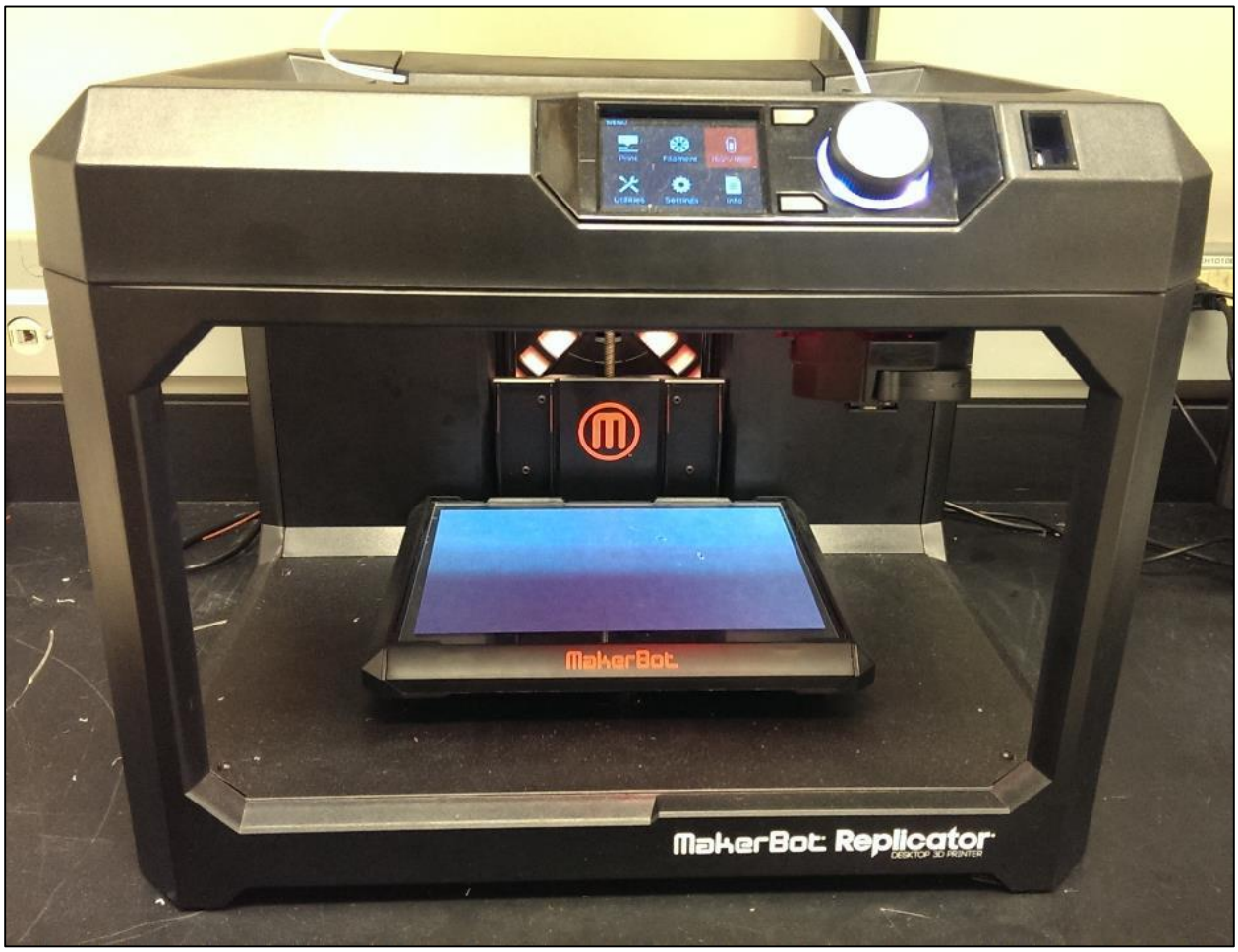

Figure 2. MakerBot 5th-Generation Replicator 3D printer used for PLA matrix manufacture.

Two types of cross-sectional geometries were considered: (a) solid cross-sections (5 mm x 15 mm) and (b) cross-sections (5 mm x 15 mm) containing three (3) equally spaced 3 mm-diameter post-tensioning ducts (see **Figure 3**). A plan view of an example dogbone PLA specimen is also provided in **Figure 4**.

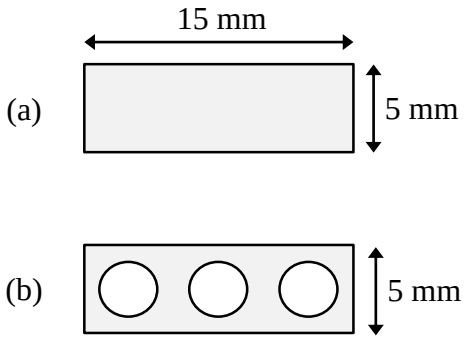

Figure 3. Cross-sectional geometries of tensile PLA dogbone specimens (a) without post-tensioning ducts and (b) with three (3) 3-mm diameter post-tensioning ducts.

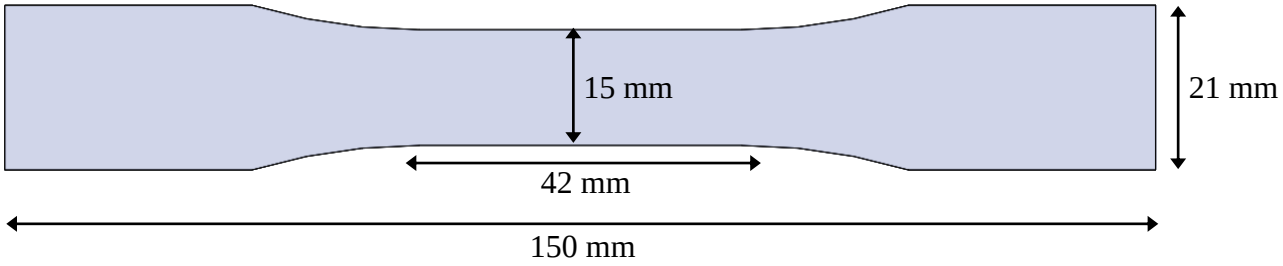

Figure 4. Plan view of tensile PLA dogbone specimen geometry.

A summary of the six (6) classes of tensile specimens is presented below in **Table 2**. Given the reduced tensile properties of jute fibers compared to flax fibers and, correspondingly, the anticipated reduced mechanical performance compared to flax-reinforced composites, only one (1) class of jute-reinforced specimens was prepared (T-J1) using a fiber prestress level of 50% of the ultimate fiber tensile strength, σ_u. Due to size limitations, one (1) jute fiber per duct (3 total strands) was used for the T-J1 specimens. Three (3) classes of flax-reinforced specimens were considered. Six (6) flax fibers per duct (18 total strands) were used for the first class (T-F1) (25% σ_u) and second class (T-F2) (50% σ_u) of flax-reinforced specimens and eight (8) flax fibers per duct (24 total strands) for the third class (T-F3) (50% σ_u) of flax-reinforced specimens.

After threading the fibers through the ducts and anchoring one end by knotting the fibers, the fibers were post-tensioned using an Instron 5869 Universal Testing Machine. One end of the specimens was affixed in the machine grips, while the fibers were fixed in the opposite grip. After pre-tensioning the fibers, the machine was paused so that 3D-printed anchors could be fitted to the free end of the specimen. These anchors ensured that the fibers were secured in their initial stressed state in order to prevent a significant loss of prestressing in the reinforcement strands. The prestressing technique is represented schematically in **Figure 5**. Examples of finished prepared tensile specimens of types T-U1, T-J1, and T-F2 are shown in **Figure 6** prior to mechanical testing.

Table 2. Tensile specimen summary indicating levels of prescribed fiber post-tensioning.

Specimen Nomenclature	Property					
	Cross-section	**Number of ducts**	**Reinforce-ment fiber**	**Number of fibers per duct**	**Number of fibers per specimen**	**Post-tension force (N, $\%\sigma_u$)**
T-S1	Solid rectangle	0	None	0	0	0
T-U1	Ducted rectangle	3	None	0	0	0
T-J1	Ducted rectangle	3	Jute	1	3	400 N, 50%
T-F1	Ducted rectangle	3	Flax	6	18	275 N, 25%
T-F2	Ducted rectangle	3	Flax	6	18	550 N, 50%
T-F3	Ducted rectangle	3	Flax	8	24	730 N, 50%

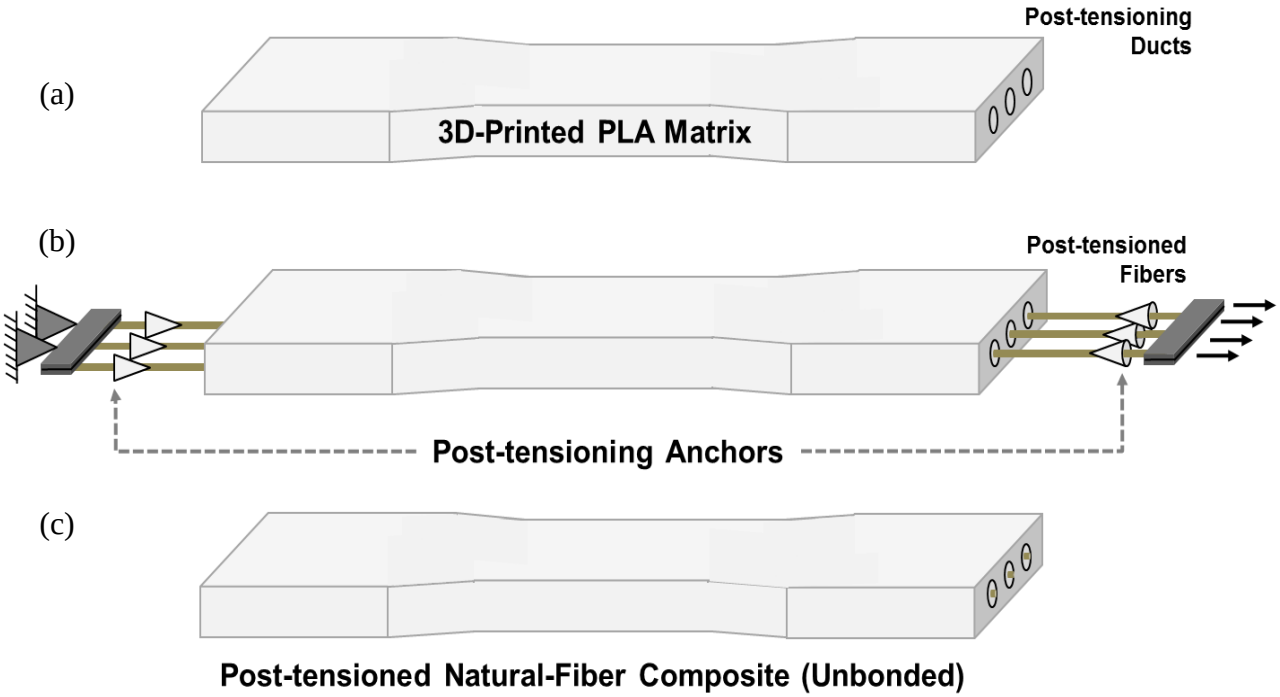

Figure 5. Schematic of the fiber post-tensioning process: (a) the PLA matrices were first 3D-printed with smooth, continuous post-tensioning ducts, (b) fibers were threaded through the ducts, anchored on one end, post-tensioned to a prescribed level of stress, and anchored into place, and (c) the fibers were released, resulting in NFCs in an initially compressed stress state.

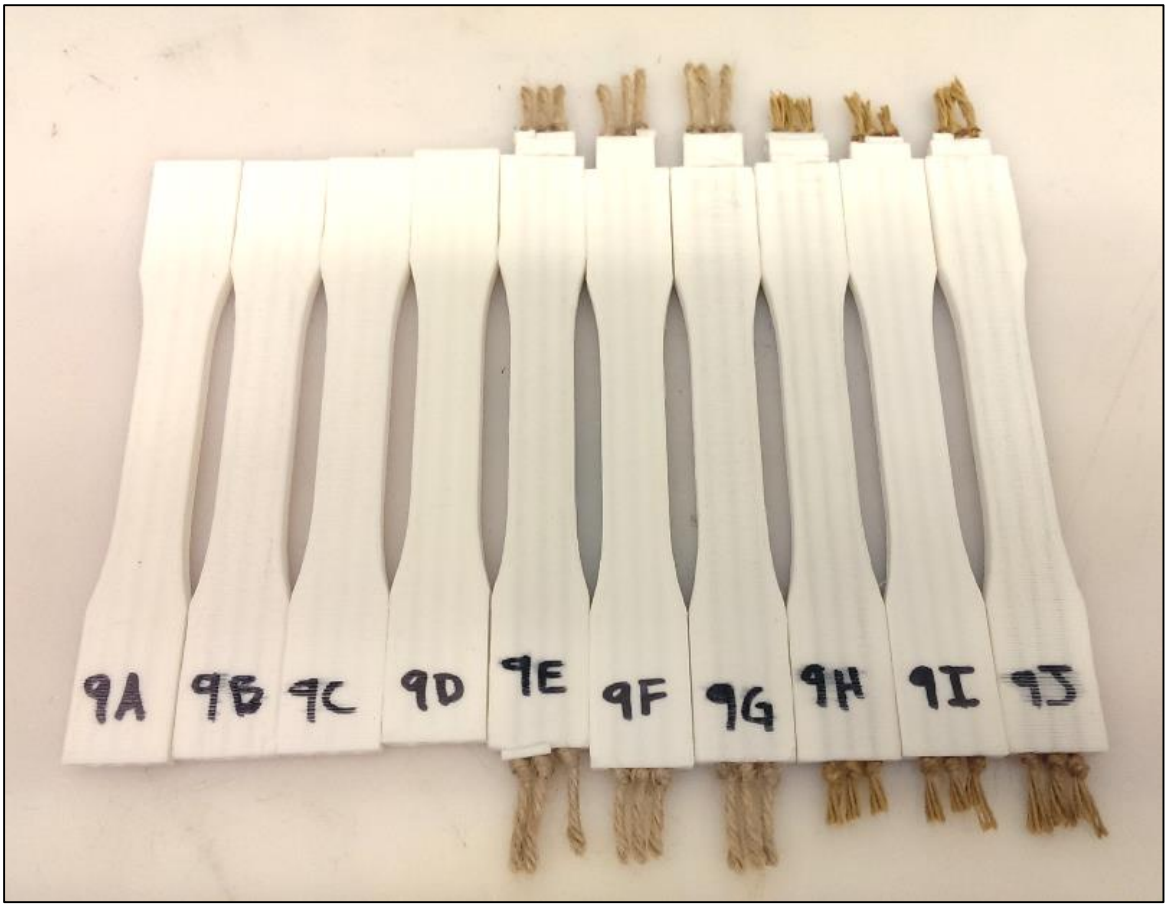

Figure 6. Prepared tensile specimen types T-U1, T-J1, and T-F3 prior to mechanical testing.

2.2.2.2 Natural fiber tensile mechanical characterization

To determine appropriate force (and stress) levels for fiber prestressing, single-fiber tensile tests were conducted using an Instron 5869 Universal Testing Machine to characterize the mechanical properties, namely tensile strength and tensile stiffness, of the individual jute and flax fiber constituents. Five (5) samples of jute and flax were tested using a displacement-control rate of 0.1 mm/s. An example of one trial of fiber strength tests (extensometer omitted) is shown in **Figure 7**. Details on calculating the ultimate tensile strength and tensile stiffness (modulus of elasticity) of each individual fiber sample have been reported elsewhere [29].

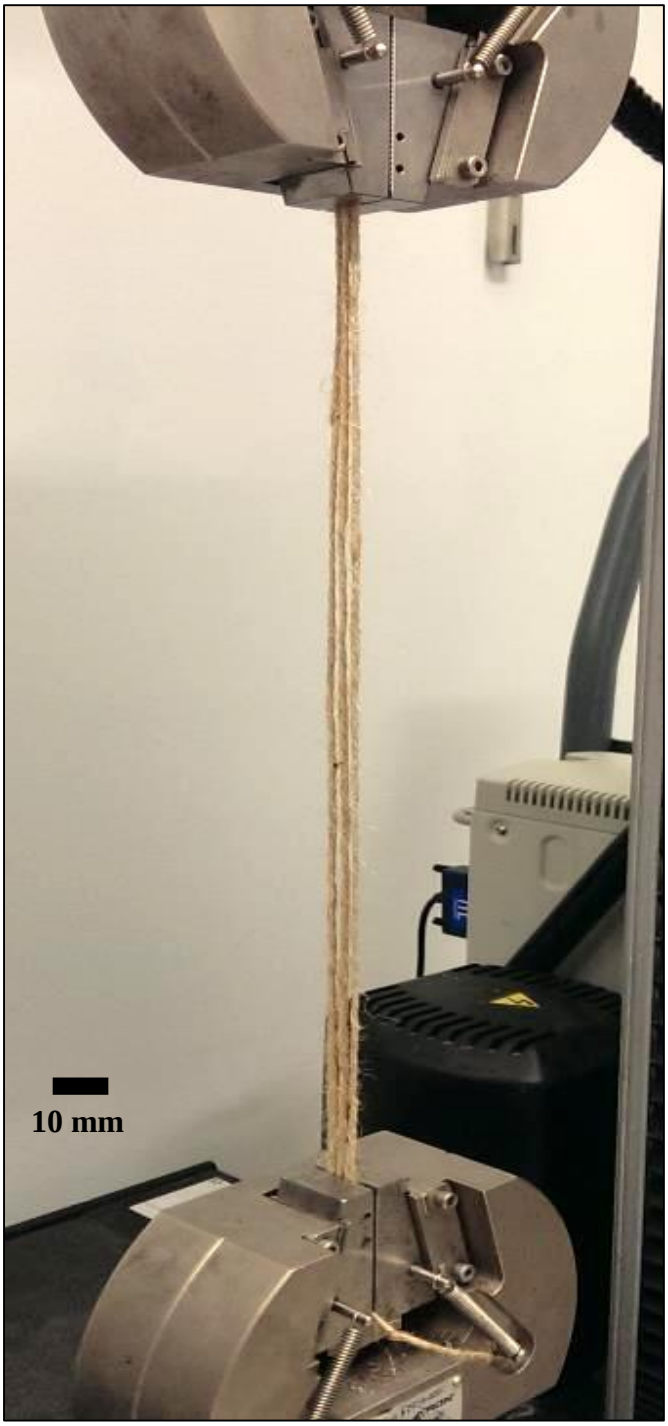

Figure 7. Sample of three (3) jute fibers during mechanical tensile strength testing.

2.2.2.3 PLA compressive mechanical characterization

To determine if a difference existed between PLA tensile strength and compressive strength, compressive mechanical tests were conducted using an Instron 5869 Universal Testing Machine in accordance with testing standard ASTM D695. Five (5) non-slender, rectangular prism samples of PLA with dimensions 12.7 mm x 12.7 mm x 25.4 mm (depicted in **Figure 8**) were tested using a displacement-control rate of 0.025 mm/s. The compressive strength (MPa) of each specimen was determined using the following equation:

$$\sigma'_c = \frac{P_1}{A}$$

where P_1 is the first peak force encountered before the plastic plateau (N) and A is the cross-sectional area (mm^2). The P_1 force can be more readily visualized by referring to the compressive force-displacement curves in Appendix A.

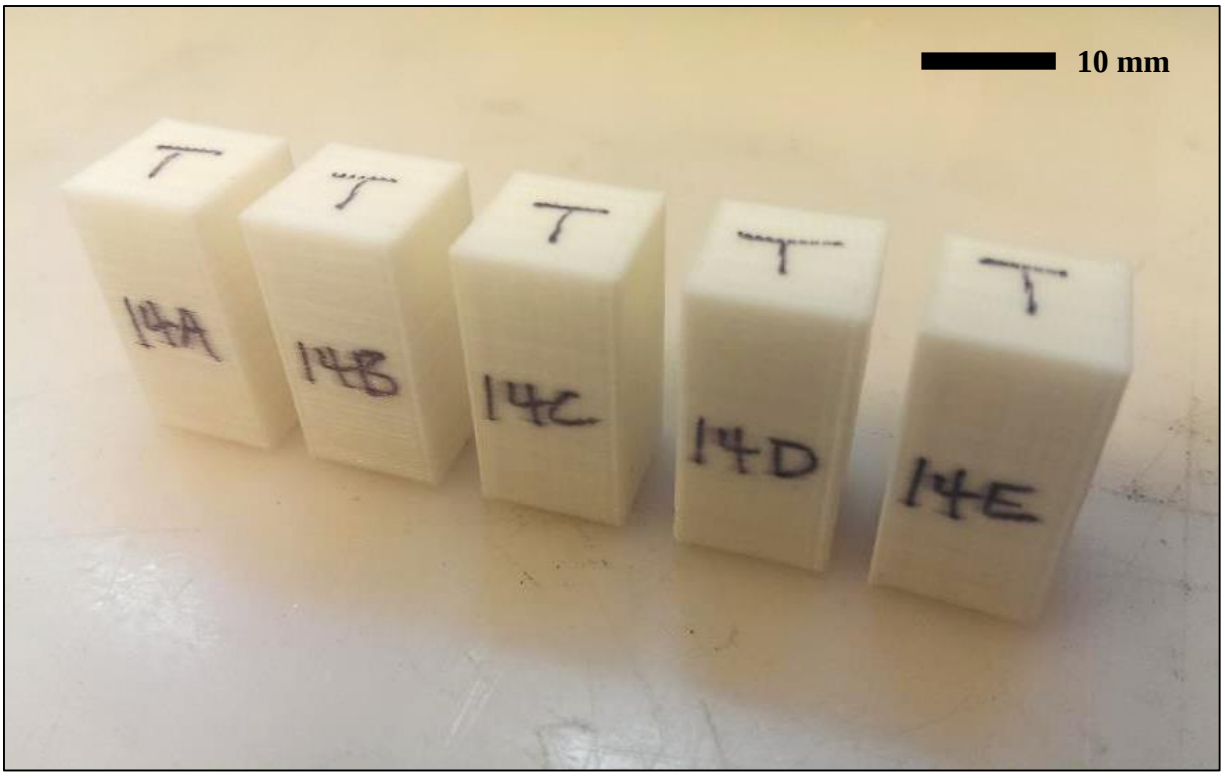

Figure 8. Rectangular prism-shaped, solid PLA compressive specimens.

2.2.2.4 PLA composite tensile mechanical characterization

All tensile composite specimens were tested using an Instron 5869 Universal Testing Machine, using a displacement rate of 0.05 mm/s. Each specimen type was tested in triplicate at minimum. **Figure 9** depicts an example photograph of one tensile specimen during mechanical testing.

Ultimate tensile strength, tensile modulus of elasticity, and weights were calculated for each specimen, from which strength- and stiffness-to-weight ratios (i.e., tensile and flexural mechanical properties normalized by specimen weight) were determined. Tensile strength-to-weight ratios (MPa/g) were calculated according to the following equation:

$$\sigma'_t = \frac{P_u}{AW}$$

where P_u is the ultimate tensile force (N), A is the cross-sectional area (mm^2), and W is the specimen weight (g). Tensile stiffness-to-weight ratios (MPa/g) for each class of tensile specimens were calculated by:

$$E'_t = \frac{CL}{AW}$$

where L is the extensometer gage length (mm) and C is the initial slope of the force-displacement curve between 10% and 40% of the ultimate peak load (N/mm).

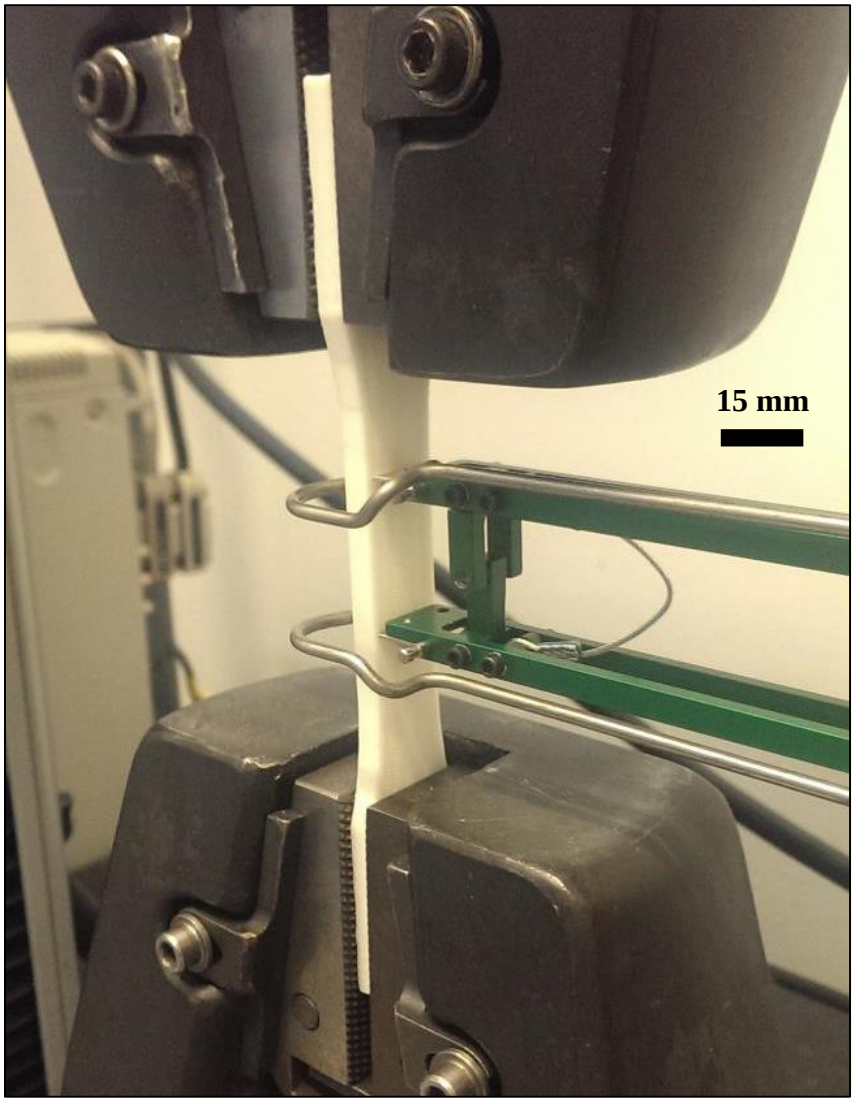

Figure 9. Tensile composite specimen during mechanical testing.

2.3 Results and Discussion

2.3.1 Single fiber tensile mechanical properties

Mechanical property (e.g., strength and stiffness) results from the single fiber tensile tests of the jute and flax fibers are shown in **Figure 10**. As expected, the results illustrate that the continuous flax fibers were stronger and stiffer than the jute fiber samples. On average, the strength and stiffness of the jute fibers were 75.0 MPa and 4380 MPa, respectively, compared to 266 MPa and 17300 MPa for the flax fibers. The fiber mechanical property values calculated in this study appear to lie below value ranges shown in some published literature sources [30,64]. It is believed that this discrepancy can be attributed to the method of calculating cross-sectional area of the fibers in this study — the use of the nominal bulk fiber strand diameter in the calculation likely produces an overestimate of fiber cross-sectional area and consequent underestimate of strength and stiffness.

Given that the flax fibers were stronger and stiffer than the jute fibers, it was anticipated that flax fibers would be more effective in a prestressed-fiber composite application. Thus, while jute fibers were included for completeness, this study focused primarily on investigating the performance of prestressed flax-reinforced PLA composites.

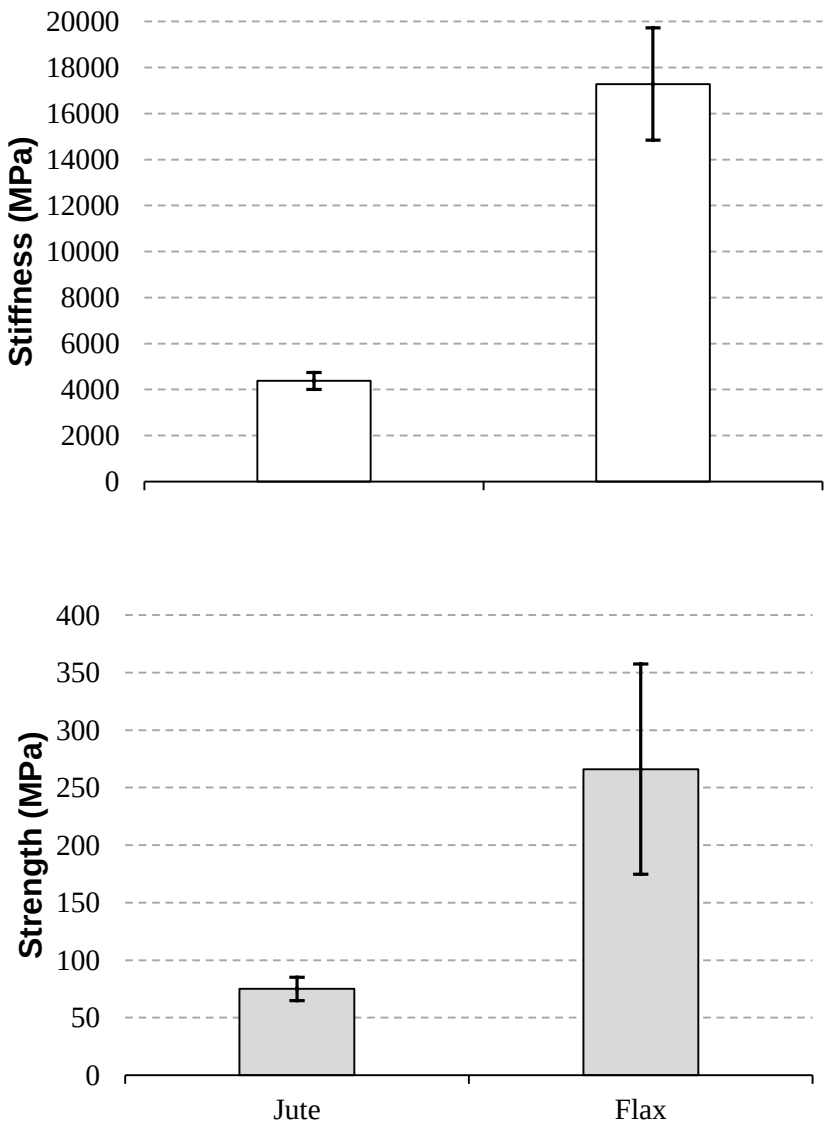

Figure 10. Average tensile strength and stiffness of jute and flax reinforcing fibers. Error bars represent ± one standard deviation.

2.3.2 PLA compressive mechanical properties

The computed average compressive strength of the solid PLA specimens was 66.0 MPa, with a standard deviation of 1.1 MPa. A comparison of this compressive strength result and the average tensile strength computed for the solid cross-section specimens in the following section (section 2.3.3) of 37.4 MPa indicates that the PLA matrix material is stronger in compression than

in tension. A visual representation of the comparison is provided in **Figure 11**. Based on these experimental results, PLA exhibits a 76% higher strength in compression than in tension.

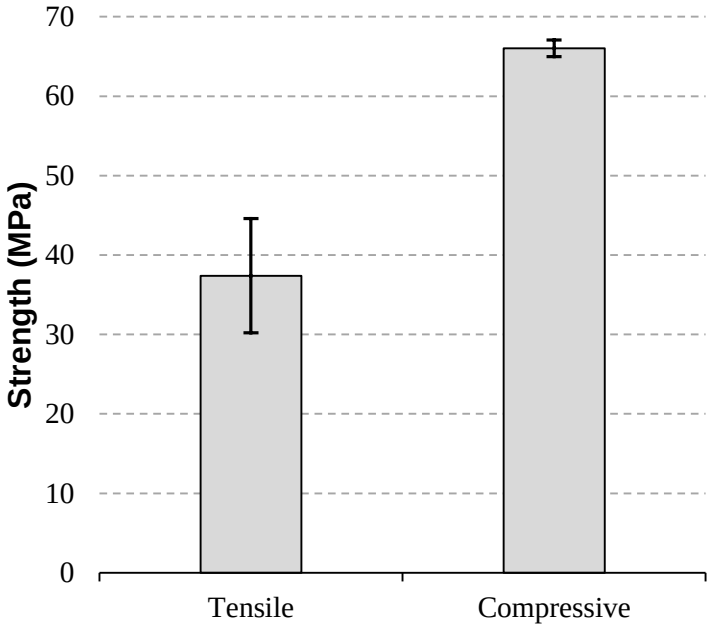

Figure 11. Comparison of experimental tensile and compressive strengths of solid PLA.

Additionally, no abrupt material failure was observed during the compressive testing — the PLA specimens continued to flatten indefinitely. **Figure 12** shows a photograph of compressive specimens before and after compressive testing. The PLA compressive behavior can also be observed more quantitatively by referring to the compressive force-displacement curves in Appendix A. The comparatively higher compressive strength and apparent ductile compressive failure mechanism of PLA suggest that the material lends itself to prestressing of fiber reinforcement in composite applications, in which the prestressing induces increased compressive forces and thus takes advantage of superior matrix compressive behavior and reduces the likelihood of brittle tensile failure.

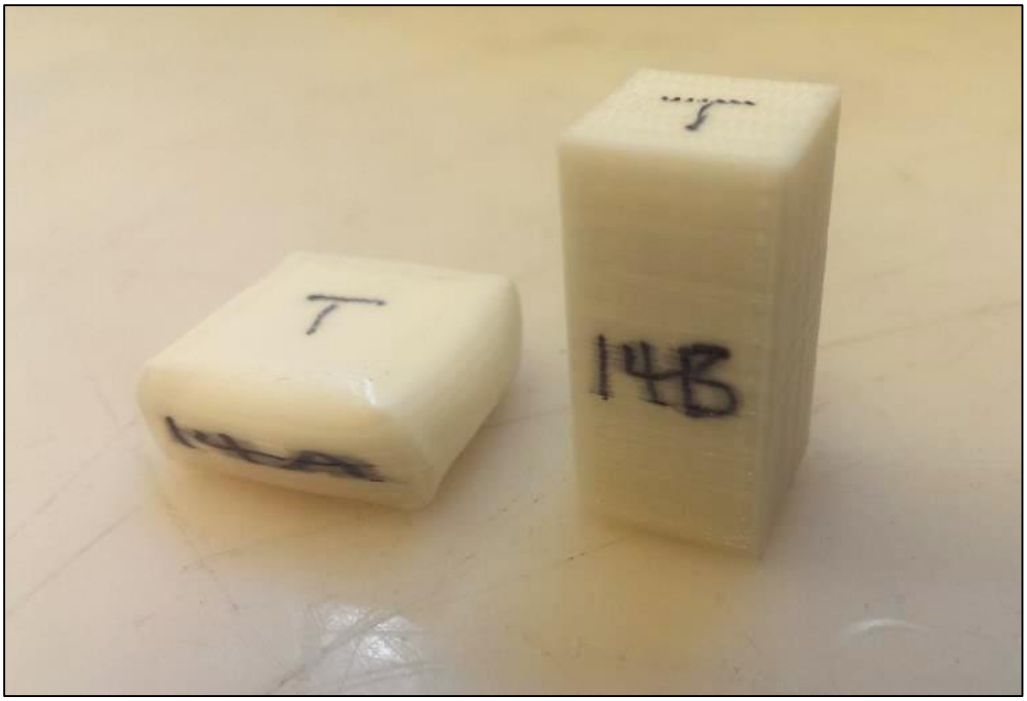

Figure 12. PLA compressive specimens before (right) and after (left) compressive mechanical testing.

2.3.3 Prestressed NFC tensile mechanical properties

Examples of post-failure tensile composite specimens are presented in **Figure 13**. Representative tensile stress-strain relationships of the ducted unstressed (T-U1), 25% prestressed flax (six strands per duct) (T-F1), and 50% prestressed flax (eight strands per duct) (T-F3) tensile specimens are shown in **Figure 14**. The stress-strain behaviors clearly demonstrate increases in ultimate tensile strength and stiffness with the incorporation of fibers from the unreinforced case (T-U1 vs. T-F1). Furthermore, it is evident from these representative stress-strain behaviors that ultimate tensile strength and stiffness are further improved with higher levels of prestressing (i.e., T-F1 vs. T-F3).

Figure 13. Flax-reinforced tensile composite specimens, post-break.

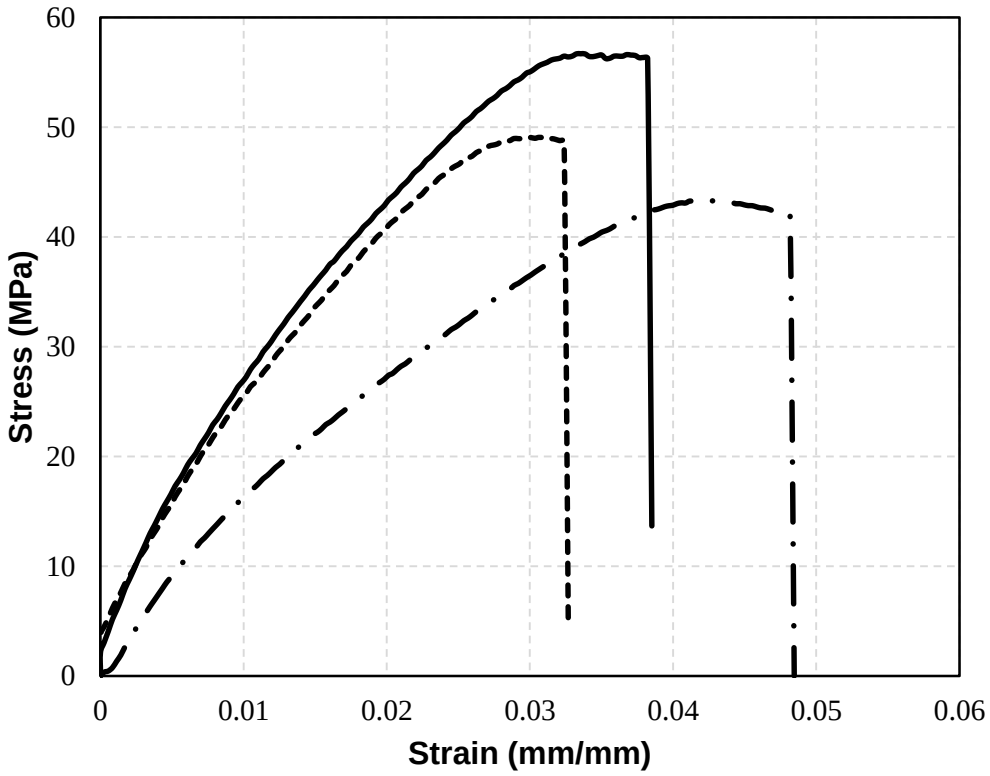

Figure 14. Representative tensile stress-strain relationships for T-U1 (— • —), T-F1 (— —), and T-F3 (—) composite specimens.

The values for ultimate tensile strength, tensile modulus, tensile strength-to-weight ratio (σ'_t), tensile stiffness-to-weight ratio (E'_t), and percent (%) increase from the solid, unreinforced PLA sample (T-S1) are presented numerically in **Table 3** and graphically in **Figure 15** for all unstressed and prestressed tensile dogbone specimens. These data indicate that all of the ducted sections (with and without fiber) result in higher specific properties than the solid PLA sample (T-S1). The increase in σ'_t and E'_t from T-S1 to the unreinforced ducted cross-section (T-U1) was approximately 64% and 30%, respectively.

Table 3. Average tensile mechanical property comparisons between the solid (T-S1), unreinforced (T-U1) and prestressed jute and flax natural fiber-reinforced PLA composites.

Specimen	Property					
	Tensile Strength, σ (MPa)	Modulus of Elasticity, E (MPa)	σ'_t (MPa/g)	% Increase (σ'_t)	E'_t (MPa/g)	% Increase (E'_t)
T-S1	37.4 ± 7.2	3053 ± 112	2.25 ± 0.39	--	184 ± 10	--
T-U1	38.8 ± 6.4	2499 ± 431	3.70 ± 0.49	64%	239 ± 35	30%
T-J1	40.8 ± 4.3	2613 ± 506	3.74 ± 0.82	66%	235 ± 42	27%
T-F1	49.7 ± 2.0	3145 ± 144	4.31 ± 0.18	92%	273 ± 14	48%
T-F2	46.4 ± 2.1	2941 ± 300	4.55 ± 0.38	104%	288 ± 37	57%
T-F3	56.3 ± 0.7	3457 ± 371	4.85 ± 0.06	116%	298 ± 32	62%

Improvements in specific properties can be seen from the unreinforced specimens (T-U1) to the prestressed jute- (T-J1) and flax-reinforced specimens (T-F1, T-F2, T-F3). As anticipated, the jute-reinforced specimens (T-J1) did not show as significant improvements in specific properties over the unreinforced case (T-U1) compared to the flax-reinforced composites. Expectedly, the T-F3 samples exhibited the highest increases in σ'_t (116%) and E'_t (62%) in comparison to the solid PLA specimens (T-S1). The flax-reinforced specimens also showed a maximum increase in σ'_t over the unreinforced ducted specimens (T-U1) from 3.70 MPa/g to 4.85 MPa/g and in E'_t from 239 MPa/g to 298 MPa/g. These improvements suggest a clear enhancement of mechanical properties with additional natural fiber prestressing.

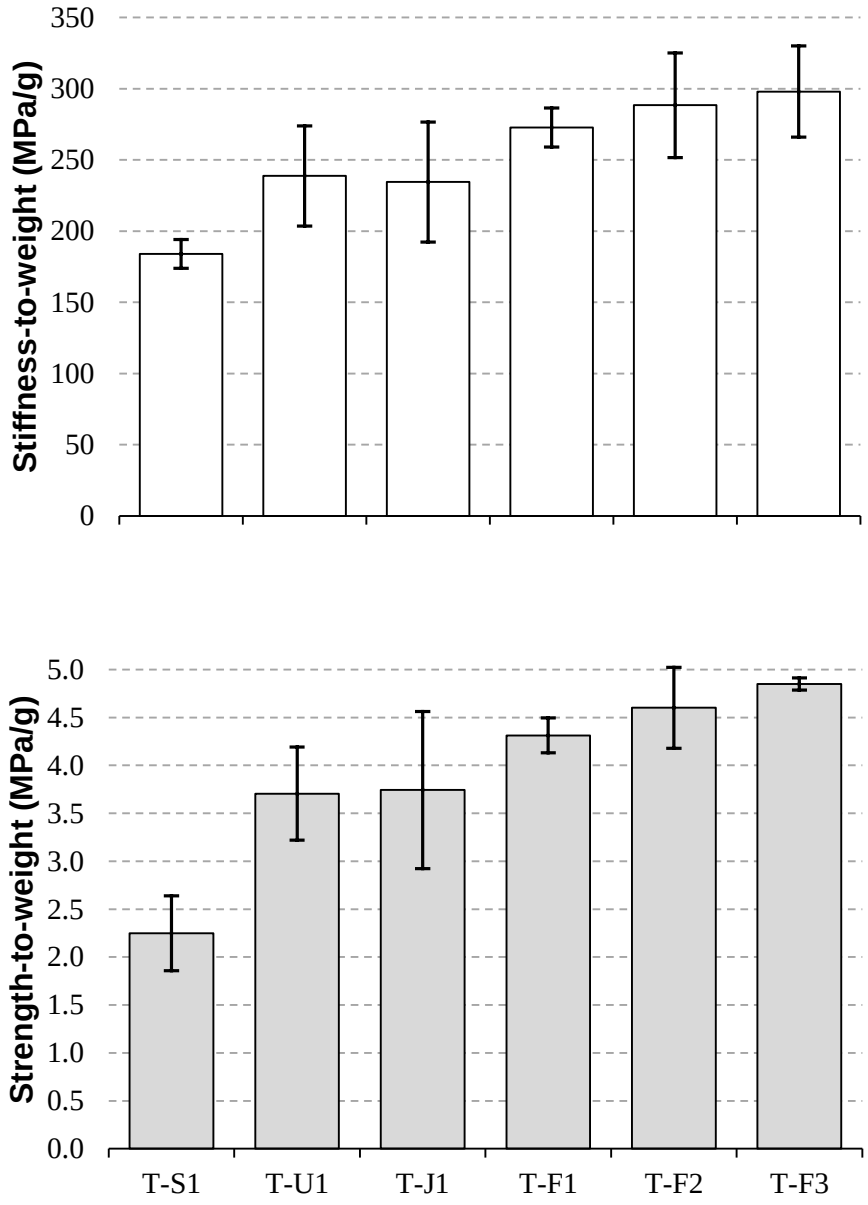

Figure 15. Specific tensile stiffness (above) and strength (below) properties of unreinforced and prestressed jute- and flax-reinforced PLA dogbone specimens.

In addition to all of the samples exhibiting statistically significant increases in both σ'_t and E'_t compared to T-S1, an analysis of variance (ANOVA) confirms that increases in σ'_t and E'_t from both the unreinforced case (T-U1) and the jute-reinforced case (T-J1) for flax-reinforced specimen groups T-F2 and T-F3 are statistically significant (p-value < 0.05). A summary of all

ANOVA specimen property comparison results is shown in **Table 4**. All specific property comparisons that yielded a statistically significant (p-value < 0.05) difference between specimen groups are highlighted in gray.

Table 4. ANOVA results summary for tensile specimen specific properties.

Property	Specimen	Compared with	p-value
σ'_t	T-S1	T-U1	0.001
		T-J1	0.016
		T-F1	0.001
		T-F2	0.000
		T-F3	0.000
	T-U1	T-J1	0.913
		T-F1	0.070
		T-F2	0.004
		T-F3	0.003
	T-J1	T-F1	0.277
		T-F2	0.038
		T-F3	0.050
	T-F1	T-F2	0.307
		T-F3	0.009
	T-F2	T-F3	0.358
E'_t	T-S1	T-U1	0.030
		T-J1	0.078
		T-F1	0.001
		T-F2	0.002
		T-F3	0.004
	T-U1	T-J1	0.829
		T-F1	0.148
		T-F2	0.025
		T-F3	0.032
	T-J1	T-F1	0.169
		T-F2	0.028
		T-F3	0.044
	T-F1	T-F2	0.510
		T-F3	0.278
	T-F2	T-F3	0.715

CHAPTER 3
Experimental Flexural Testing

3.1 Overview

PLA specimens of six (6) cross-sectional geometries were manufactured for experimental flexural testing. Solid, unreinforced, and prestressed fiber-reinforced composite PLA flexural specimens of rectangular and I-shape cross-sections were prepared after experimental tensile testing and subsequent mechanical characterization of two types of natural fibers was performed. The PLA and fiber-reinforced PLA flexural specimens were then experimentally tested in order to characterize mechanical properties and response. Results for specific (weight-normalized) mechanical properties were calculated from the experimental testing data for each specimen type and compared between groups to determine the influence of cross-sectional geometry and fiber reinforcement on mechanical properties.

Flexural testing was separated into three (3) primary trials. The objective of Trials 1 and 2 was to determine the effect of cross-sectional geometry, fiber reinforcement, and quantity of reinforcement on mechanical properties. The objective of Trial 3 was to isolate the effect of only fiber reinforcement prestressing on mechanical properties. In Trials 1 and 2, an initial, preliminary prestressing fiber anchorage technique was employed. In Trial 3, the anchorage technique was refined and improved by 3D printing anchors that demonstrated more rigidity and adequate fit.

3.2 Materials and Experimental Methods

3.2.1 Materials

Natural jute fibers (2.0 mm diameter) and flax fibers (0.5 mm diameter) were commercially obtained from a local hardware supply store. Polylactic acid (PLA) was supplied in spooled filament form (1.8 mm diameter) by MakerBot Industries, LLC.

3.2.2 Experimental methods

3.2.2.1 Flexural specimen manufacture and preparation

Similar to the tensile composite specimens, flexural PLA matrices were computer-modeled and 3D-printed using a MakerBot 5th-Generation Replicator Desktop 3D printer. The extruder temperature, resolution, and print speed were also set to 215 °C, 0.2 mm, and 60 mm/s, respectively. The 3D printer used to manufacture the PLA matrices can be seen in **Figure 2**.

Using the six (6) cross-sections illustrated in **Figure 16**, a total of nine (9) flexural specimen types were prepared. The flexural specimen types are summarized in **Table 5**. Specimens were designed to have rectangular, ducted rectangular, I-shape, and ducted I-shape cross-sectional geometries (see **Figure 16**). The various flexural specimen types were subject to differing degrees of post-tensioning force (see **Table 5**).

All cross-sections had nominal depths of 25 mm and widths of 15 mm, with the I-shape cross-sections having 5 mm flange and web thicknesses. Post-tensioning ducts were 3 mm in diameter and were evenly spaced within the tension side of the flexural cross-section. After 3D printing, the same fiber threading, prestressing, and anchoring technique used to fabricate the prestressed tensile specimens was employed. The prestressing technique for the flexural beam specimens is shown schematically in **Figure 17**.

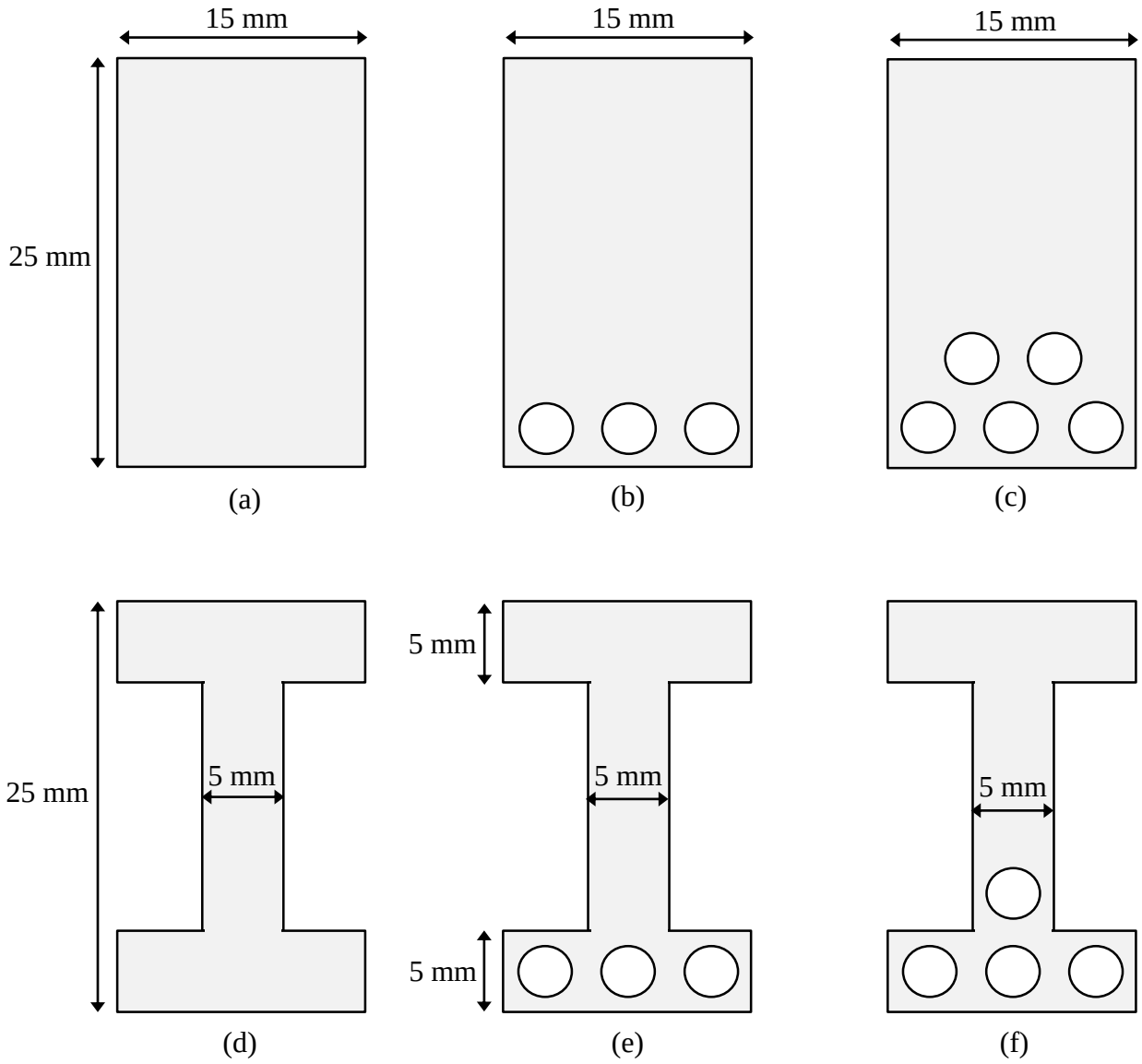

Figure 16. Cross-sectional geometries of flexural PLA specimens: (a) solid rectangular, (b) rectangular with three (3) 3-mm diameter post-tensioning ducts, (c) rectangular with five (5) ducts, (d) solid I-shape, (e) I-shape with three (3) ducts, and (f) I-shape with four (4) ducts.

As shown in **Table 5**, four (4) classes of jute-reinforced flexural specimens (1 strand per duct) were prestressed to the same level of prestressing (50% σ_u) as the jute-reinforced tensile specimens. Two (2) classes of flax-reinforced I-beam specimens (8 strands per duct) were stressed to prescribed prestress levels of 25% (F-I-F1) and 50% (F-I-F2), respectively.

Table 5. Flexural specimen summary indicating levels of prescribed fiber post-tensioning.

Specimen Nomenclature	Property					
	Cross-section	**Number of ducts**	**Reinforce-ment fiber**	**Number of fibers per duct**	**Number of fibers per specimen**	**Post-tension force (N, %σ_u)**
F-R-S1	Solid rectangle	0	None	0	0	0
F-I-S1	Solid I-shape	0	None	0	0	0
F-I-U1	Ducted I-shape	3	None	0	0	0
F-R-J1	Ducted rectangle	3	Jute	1	3	400 N, 50%
F-R-J2	Ducted rectangle	5	Jute	1	3	667 N, 50%
F-I-J1	Ducted I-shape	3	Jute	1	3	400 N, 50%
F-I-J2	Ducted I-shape	4	Jute	1	3	533 N, 50%
F-I-F1	Ducted I-shape	3	Flax	8	24	365 N, 25%
F-I-F2	Ducted I-shape	3	Flax	8	24	730 N, 50%

The flexural composite specimens were further divided into three groups, each corresponding to a separate experiment. The three trial groups are summarized in **Table 6**, which

indicates total specimen lengths, spans lengths, and specimen types (from **Table 5**) that were tested in each experiment. Trials 1 and 2 were designed to determine the contributions of both cross-sectional geometry and jute fiber reinforcement prestressing to the improvement of mechanical properties. Trials 1 and 2 both tested a total of six (6) composite specimens.

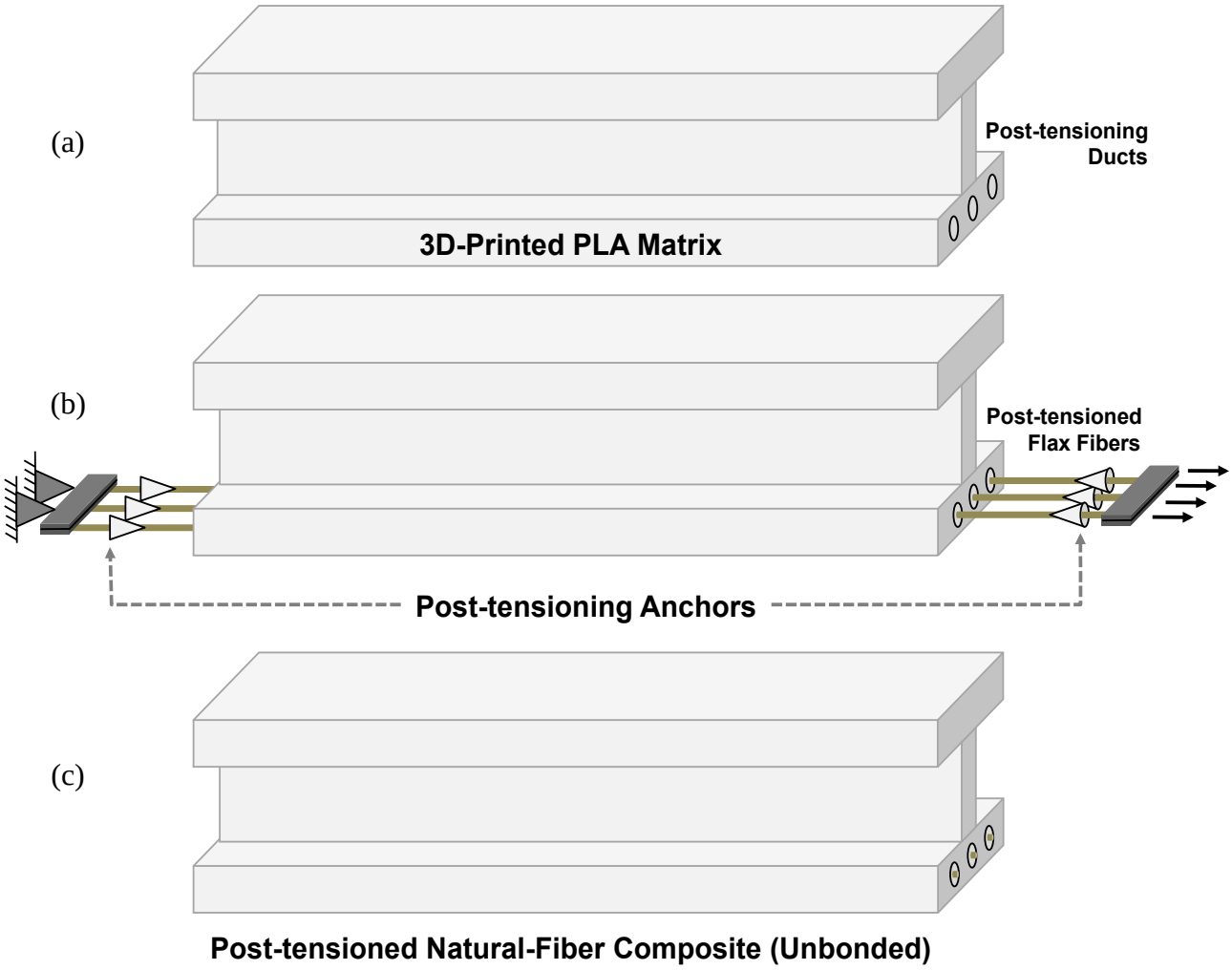

Figure 17. Schematic of the fiber post-tensioning process: (a) the PLA matrices were first 3D-printed with smooth, continuous post-tensioning ducts, (b) fibers were threaded through the ducts, anchored on one end, post-tensioned to a prescribed level of stress, and anchored into place, and (c) the fibers were released, resulting in NFCs in an initially compressed stress state.

Table 6. Summary of the three (3) primary flexural trials.

Trial	Total specimen length (mm)	Span length (mm)	Specimen types
1	140	110	F-R-S1 F-R-J1 F-I-J1
	165	135	F-R-S1 F-R-J1 F-I-J1
2	165	135	F-R-S1 F-R-J1 F-R-J2 F-I-S1 F-I-J1 F-I-J2
3	190	160	F-I-S1 F-I-U1 F-I-J1 F-I-F1 F-I-F2

Trial 3 was designed to isolate the contribution of only jute and flax fiber reinforcement prestressing. Each of the five (5) specimen types in Trial 3 was tested in triplicate, resulting in a total composite flexural specimen count of 15. Trial 3 also utilized an improved prestressed fiber anchorage technique to increase the rigidity of the anchorage and consequently reduce prestress loss. Examples of finished prepared flexural specimens of type F-I-F3 are shown prior to mechanical testing in **Figure 18**. Other finished composite specimen types were similar.

3.2.2.2 PLA composite flexural mechanical characterization

All composite specimens were tested using an Instron 5869 Universal Testing Machine. The flexural specimens were tested in three-point bending using a displacement rate of 0.05 mm/s. **Figure 19** shows an example photograph of one flexural specimen during mechanical testing.

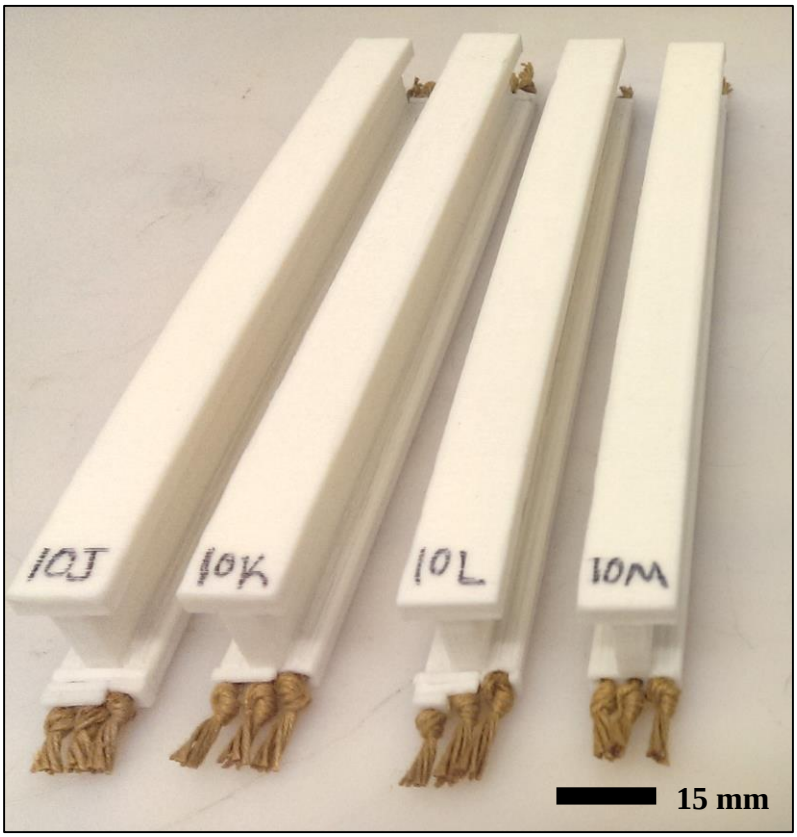

Figure 18. Flexural composite specimens of type F-I-F2 prior to mechanical testing.

Flexural strength- and stiffness-to-weight ratios were calculated for each flexural composite specimen. Flexural strength-to-weight ratios (MPa/g) were calculated according to the following equation:

$$\sigma'_f = \frac{P_u L h}{8 W I}$$

where P_u is the ultimate peak midspan force (N), L is the span length (mm), h is the depth of the cross-section (mm), W is the weight of the specimen (g), and I is the moment of inertia of the cross-section (mm^4).

Flexural stiffness-to-weight ratios (MPa/g) were calculated using the following linear-elastic relationship:

$$E'_f = \frac{CL^3}{48WI}$$

where C was determined using a similar chord technique as with the tensile specimens (N/mm).

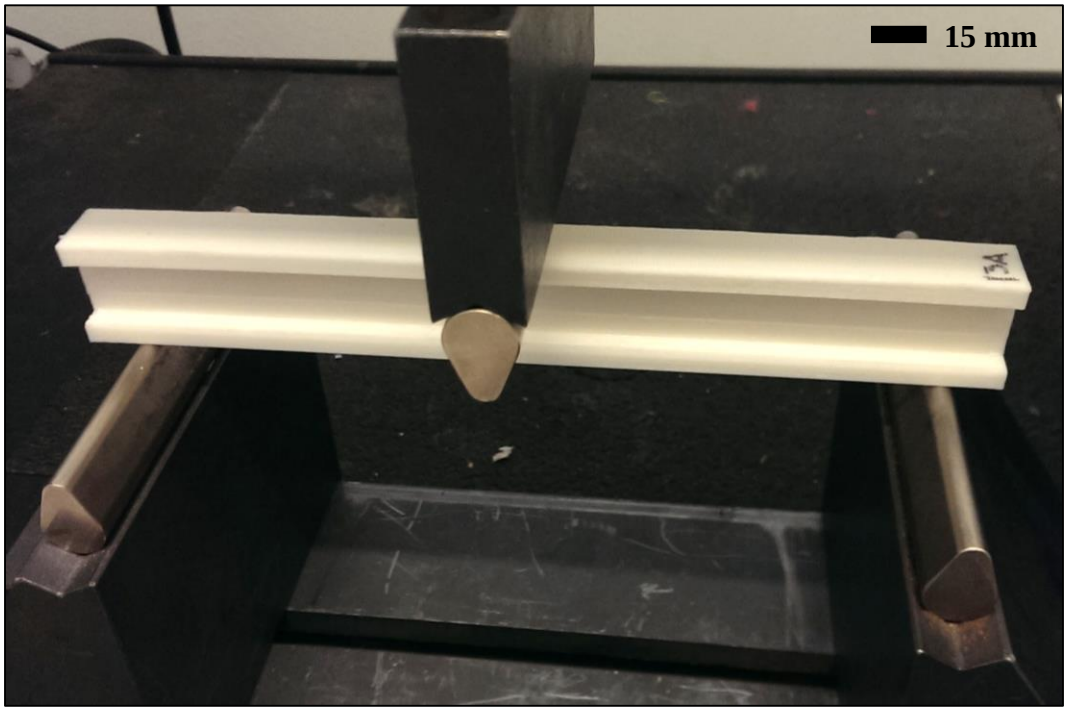

Figure 19. Flexural specimen during three-point bending mechanical testing.

3.3 Results and discussion

3.3.1 Flexural mechanical properties of prestressed NFCs

3.3.1.1 Trial 1 – Effects of cross-sectional geometry and addition of jute fibers

As mentioned previously, Trial 1 was designed to determine the effects of cross-sectional geometry and jute fiber reinforcement prestressing on mechanical properties of the flexural composite specimens. Trial 1 included three (3) specimen types: solid rectangle, jute-reinforced rectangle, and jute-reinforced I-shape (F-R-S1, F-R-J1, F-I-J1). Two span lengths (110 mm and 135 mm) were used for each type, resulting in six total flexural composite specimens. The specific mechanical property results for Trial 1 are presented below in **Figure 20**.

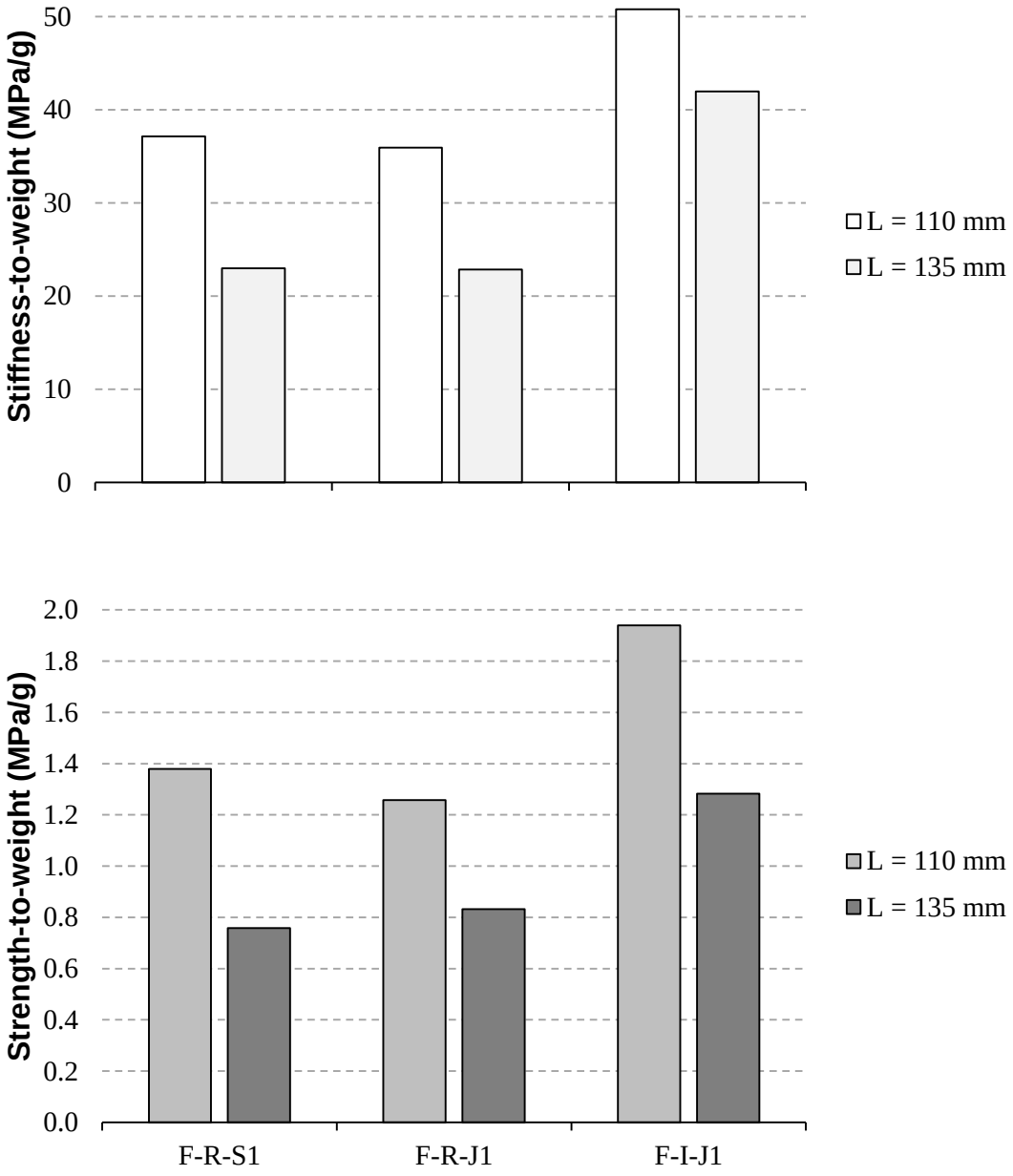

Figure 20. Specific flexural mechanical property results for Trial 1.

For both span lengths, the I-shape cross-section (F-I-J1) exhibited higher strength-to-weight and stiffness-to-weight ratios compared to both of the rectangular cross-sections (F-R-S1 and F-R-J1). Strength-to-weight ratios for 110 mm- and 135 mm-span I-shape specimens were

1.94 and 1.28 MPa/g, respectively, compared to ratios of 1.38 and 0.76 MPa/g for the solid rectangular and 1.26 and 0.83 MPa/g for the jute-reinforced rectangular specimens. Similarly, stiffness-to-weight ratios for 110 mm- and 135 mm-span I-shape specimens were 50.8 and 42.0 MPa/g, respectively, compared to ratios of 37.1 and 23.0 MPa/g for the solid rectangular and 35.9 and 22.9 MPa/g for the jute-reinforced rectangular specimens. These results demonstrate that modification of cross-sectional geometry is effective in improving specific mechanical properties.

Improvement in specific flexural mechanical properties from the solid rectangular cross-section (F-R-S1) to the jute-reinforced rectangular cross-section (F-R-J1) was not evident, which suggests the prestressed jute reinforcement was not effective in this experiment. This lack of improvement is likely attributable to the potential loss of fiber post-tensioning force prior to testing. The overall reduced specific flexural mechanical properties of the 135 mm-span set of specimens compared to the 110 mm-span set was due to the greater weights of the 135 mm-span specimens.

3.3.1.2 Trial 2 – Effects of cross-sectional geometry, addition of jute fiber, and number of fibers

As mentioned previously, Trial 2 was designed to determine the effects of cross-sectional geometry, jute fiber reinforcement prestressing, and number of jute reinforcement fibers on mechanical properties of the flexural specimens. Trial 2 incorporated six (6) specimen types: solid rectangle, jute-reinforced rectangle (3 ducts), jute-reinforced rectangle (5 ducts), solid I-shape, jute-reinforced I-shape (3 ducts), and jute-reinforced I-shape (4 ducts) (F-R-S1, F-R-J1, F-R-J2, F-I-S1, F-I-J1, F-I-J2). One composite specimen was produced for each specimen type, resulting

in six (6) total flexural composite specimens. The specific flexural mechanical property results for Trial 2 are presented in **Figure 21**.

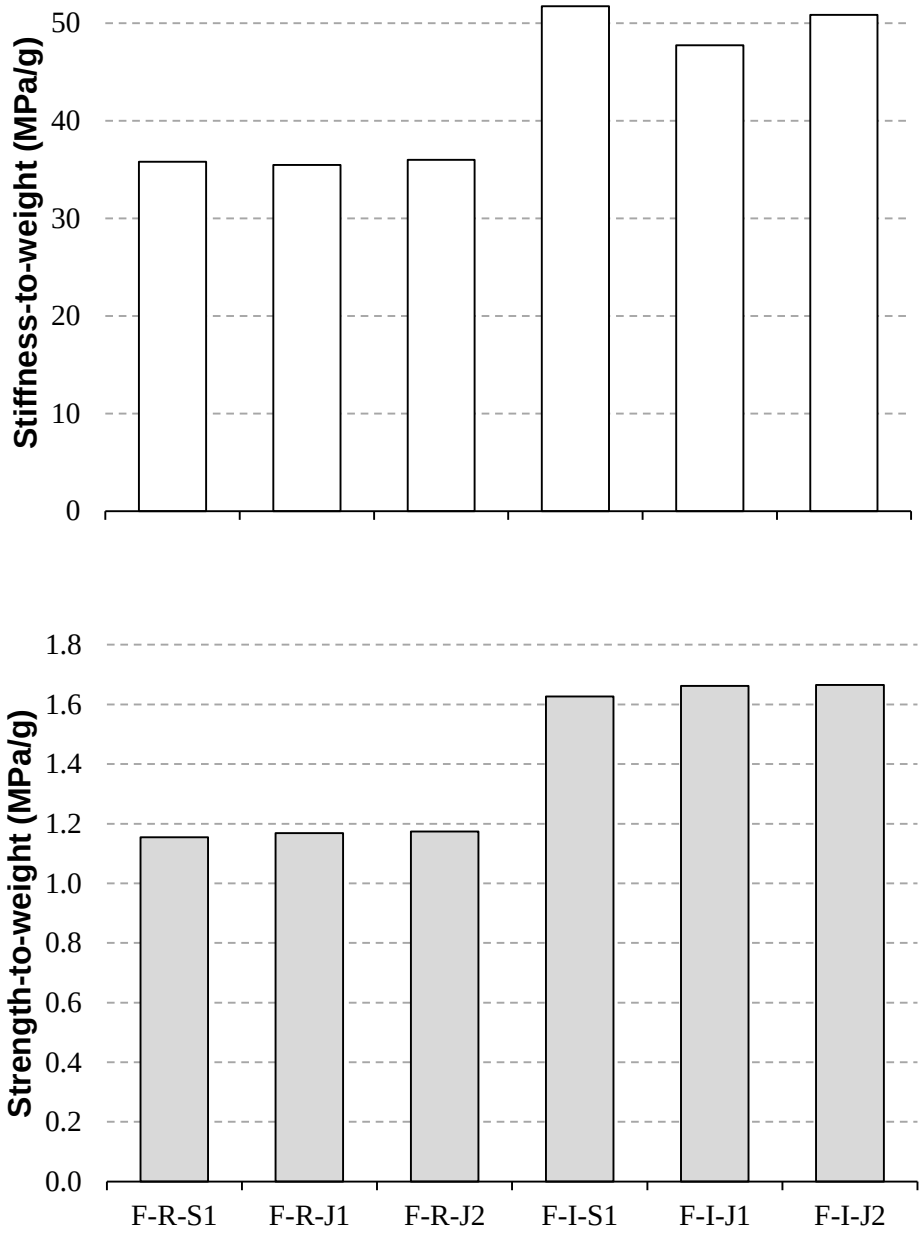

Figure 21. Specific flexural mechanical property results for Trial 2.

Similar to the results from Trial 1, the three I-shape cross-sections exhibited increased strength-to-weight and stiffness-to-weight ratios compared to the three rectangular cross-sections. Strength-to-weight ratios for the three rectangular cross-sections were 1.15, 1.17, and 1.17 MPa/g compared to 1.63, 1.66, and 1.67 MPa/g for the three I-shape cross-sections. Exhibiting a similar trend, stiffness-to-weight ratios were 35.8, 35.5, and 36.0 MPa/g for the three rectangular cross-sections compared to 51.7, 47.7, and 50.8 MPa/g for the three I-shape cross-sections. These data indicate a clear improvement in specific flexural mechanical properties from rectangular to I-shape cross-sectional geometry.

Also similar to Trial 1, however, the effect of the addition of prestressed jute reinforcement fibers did not appear to improve specific flexural mechanical properties for either rectangular or I-shape cross-sections, even considering the specimen types with a higher number of prestressed fibers in them (F-R-J2 and F-I-J2). These results suggest that in this trial, the prestressed jute fiber reinforcement was again not effective.

3.3.1.3 Trial 3 – Isolation of fiber prestressing effects

Since Trials 1 and 2 effectively demonstrated improvement in specific flexural mechanical properties due to modifications in cross-sectional geometry but not due to fiber prestressing, Trial 3 was designed to isolate improvements due to reinforcing fiber prestressing only. Only I-shape cross-sections were used in Trial 3 (three of each specimen type), and fiber reinforcement and degree of post-tensioning were varied. An improved fiber anchorage technique was used in Trial 3, in which more precise and rigid anchors were 3D printed to fit the faces of the flexural specimen flanges near the fiber ducts more adequately.

Figure 22. Flexural composite specimens post-break.

Representative flexural force-displacement relationships of the unstressed (F-I-U1), prestressed jute (F-I-J1), and prestressed flax (F-I-F2) flexural specimens are shown in **Figure 23**. The force-displacement behaviors clearly demonstrate increases in ultimate flexural strength and stiffness with the incorporation of fibers from the unreinforced case (F-I-U1 vs. F-I-J1). Moreover, it is evident from these force-displacement behaviors that ultimate flexural strength and stiffness are further improved with higher levels of prestressing (i.e., F-I-J1 vs. F-I-F2).

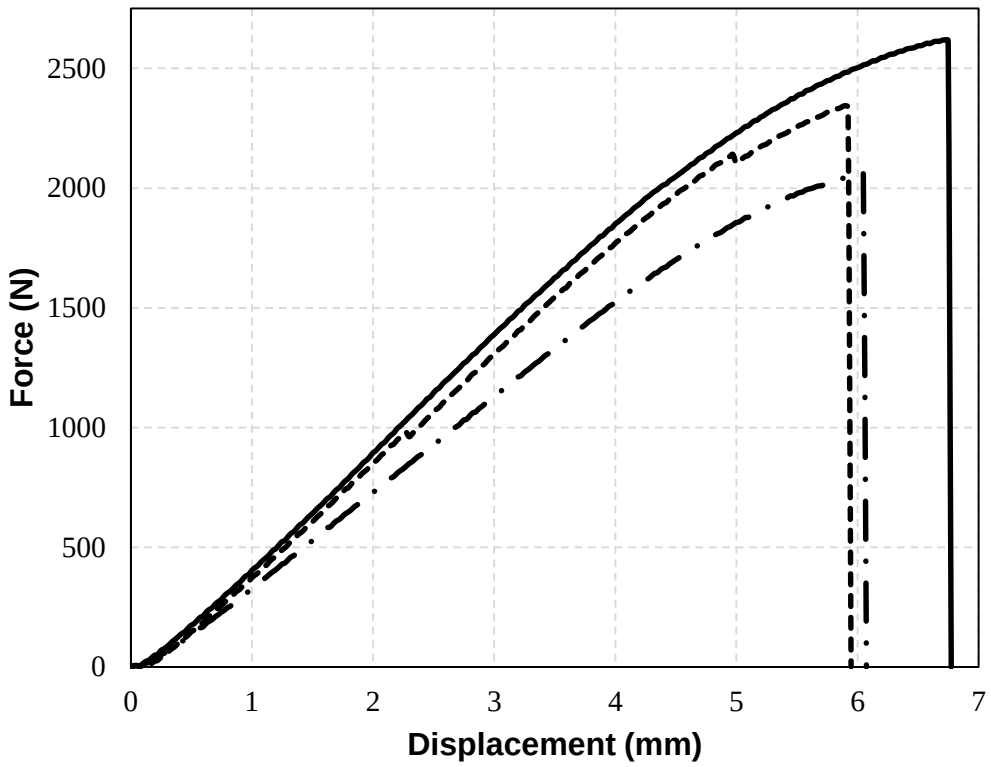

Figure 23. Representative flexural force-displacement relationships for F-I-U1 (— • —), F-I-J1 (— —), and F-I-F2 (—) composite specimens.

Results from the flexural mechanical characterization of the unreinforced, prestressed jute-fiber, and prestressed flax-fiber composite I-beams are presented numerically in **Table 7** and graphically in **Figure 24**. Similar to the tensile data, the results indicate that both the jute- and flax-reinforced specimens resulted in increases in specific flexural strength (σ'_f) and specific flexural stiffness (E'_f) compared to the unreinforced case and that these increases were further improved with higher levels of prestressing.

Table 7. Average flexural mechanical property comparisons between the unreinforced (F-I-S1) and prestressed jute and flax natural fiber-reinforced PLA composites tested in Trial 3.

Specimen	Property					
	Flexural Strength, σ (MPa)	Flexural Modulus, E (MPa)	σ'_f (MPa/g)	% Increase (σ'_f)	E'_f (MPa/g)	% Increase (E'_f)
F-I-S1	68.8 ± 3.2	2260 ± 29	1.37 ± 0.06	--	45.1 ± 0.3	--
F-I-U1	68.2 ± 9.6	2315 ± 342	1.49 ± 0.09	8%	50.5 ± 3.0	12%
F-I-J1	78.6 ± 6.9	2612 ± 168	1.68 ± 0.06	22%	55.8 ± 0.7	24%
F-I-F1	74.0 ± 1.1	2293 ± 81	1.64 ± 0.03	19%	50.7 ± 1.9	12%
F-I-F2	81.8 ± 4.0	2629 ± 128	1.81 ± 0.05	32%	58.3 ± 2.3	29%

The jute-reinforced case (F-I-J1) exhibited a 22% and 24% increase in σ'_f and E'_f, respectively, over the unreinforced case (F-I-S1). As anticipated, however, the F-I-F2 specimens demonstrated the largest increase in specific flexural mechanical properties. The F-I-F2 samples exhibited a σ'_f of 1.81 MPa/g and E'_f of 58.3 (MPa/g), which corresponded to a 32% and a 29% increase over the F-I-S1 samples, respectively. Specimen type F-I-F1 exhibited improvements of 19% and 12% in σ'_f and E'_f, respectively, over the unreinforced case (F-I-S1). The lesser improvements exhibited by F-I-F1 are likely attributable to the lower level of prestressing and to the potential losses of fiber post-tensioning force prior to testing.

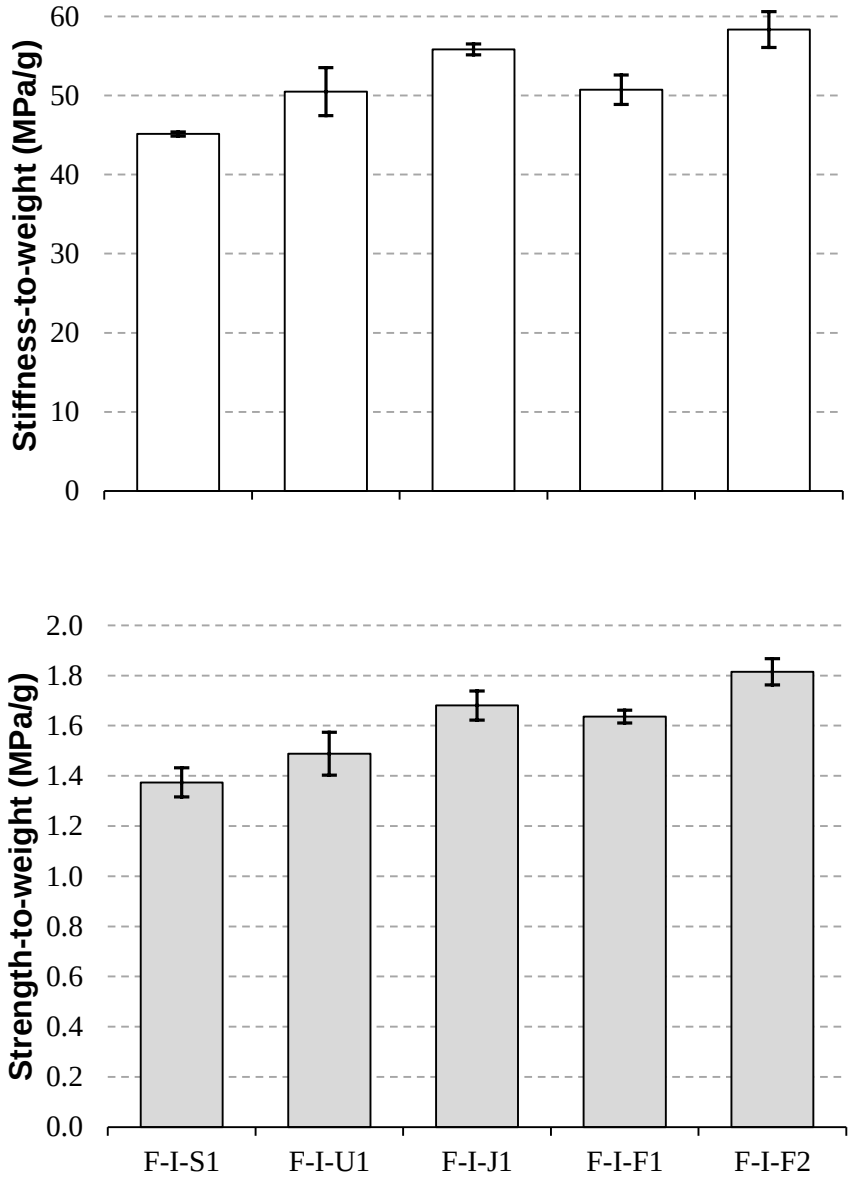

Figure 24. Specific flexural strength and stiffness properties of unreinforced and prestressed jute- and flax-reinforced PLA I-beams tested in Trial 3.

ANOVA results (summarized in **Table 8**) indicate that the increases in σ'_f and E'_f from the solid I-shape (F-I-S1) to all three fiber-reinforced cases are statistically significant (p-value < 0.05). Additionally, increases in σ'_f and E'_f from the unreinforced case (F-I-U1) to the F-I-J1 and F-I-F2, as well as between the F-I-F1 and F-I-F2 specimens samples, were statistically significant.

All specific property comparisons that yielded a statistically significant (p-value < 0.05) difference between specimen groups are highlighted in gray in **Table 8**. Therefore, the results from the flexural tests, which were designed to isolate the effect of fiber prestressing, offer conclusive evidence that the specific mechanical properties of 3-D printed PLA matrices can be improved with higher degrees of initial fiber prestressing.

Table 8. ANOVA results summary for flexural specimen specific properties from Trial 3.

Property	Specimen	Compared with	p-value
σ'_f	F-I-S1	F-I-U1	0.128
		F-I-J1	0.003
		F-I-F1	0.002
		F-I-F2	0.001
	F-I-U1	F-I-J1	0.032
		F-I-F1	0.045
		F-I-F2	0.005
	F-I-J1	F-I-F1	0.298
		F-I-F2	0.041
	F-I-F1	F-I-F2	0.006
E'_f	F-I-S1	F-I-U1	0.038
		F-I-J1	0.000
		F-I-F1	0.007
		F-I-F2	0.001
	F-I-U1	F-I-J1	0.040
		F-I-F1	0.909
		F-I-F2	0.023
	F-I-J1	F-I-F1	0.011
		F-I-F2	0.143
	F-I-F1	F-I-F2	0.011

CHAPTER 4
Modeling

4.1 Overview

Numerical and analytical models were developed in this study to compare with the experimental testing results. The first models produced were numerical finite element models of two of the flexural specimen types discussed in Chapter 3. The experimental three-point bending tests were simulated using finite element models for the unreinforced ducted I-shape (F-I-U1) and prestressed flax-reinforced I-shape (F-I-F2) specimen types. The objective of the finite element modeling was to produce flexural composite three-point bending behavior results comparable to the experimental three-point bending results. Second, analytical models in the form of predictive equations were developed to predict strength- and stiffness-to-weight ratios for the prestressed tensile composite specimens (discussed in Chapter 2). The mechanical property results from the analytical equations and from the experimental tests are then compared and discussed herein.

4.2 Finite Element Modeling

4.2.1 Methods

Utilizing the commercial finite element analysis software Abaqus, finite element models were created for the 160 mm-span (190 mm total length) F-I-U1 and F-I-F2 specimen types. Automatic seed generation was used for both models with an approximate element size of 2.5 mm. The software produced a smaller mesh size around each of the circular ducts in the tension flanges of the I-shapes. Eight-noded, 3D solid isotropic elements were used throughout both models. The finite element mesh used in both models is illustrated in **Figure 25**.

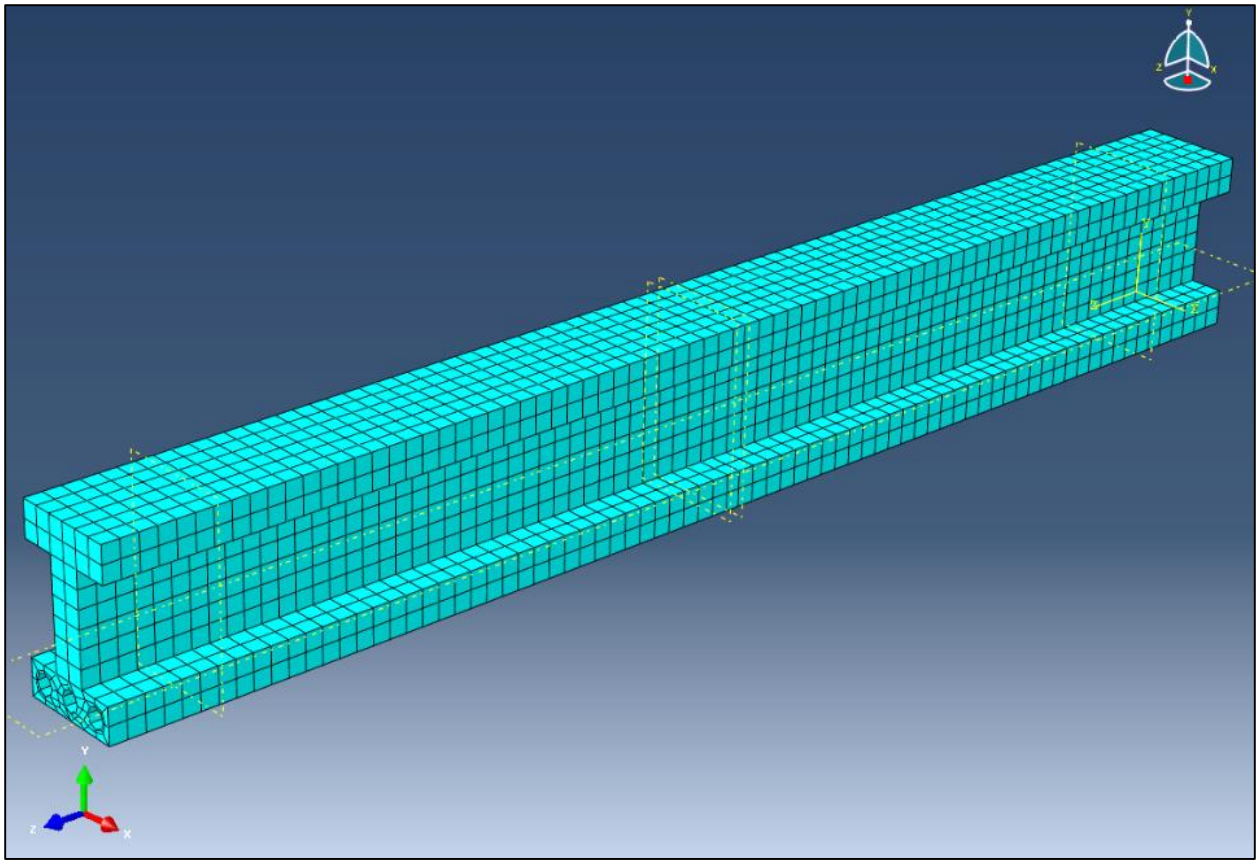

Figure 25. 3D finite element mesh of ducted I-shape specimen model, created with Abaqus software.

The constitutive relationship for PLA applied to the model included elastic and plastic behavior, as well as failure at a given strain, using values within ranges reported by the literature [11,65-67]. The stress-strain relationship that was input into the model for the PLA matrix material is displayed in **Figure 26**. This stress-strain relationship was used for both tensile and compressive behavior of PLA in each model — differences between tensile mechanical properties and compressive mechanical properties (i.e., anisotropy) were not implemented in the constitutive relationship of the models.

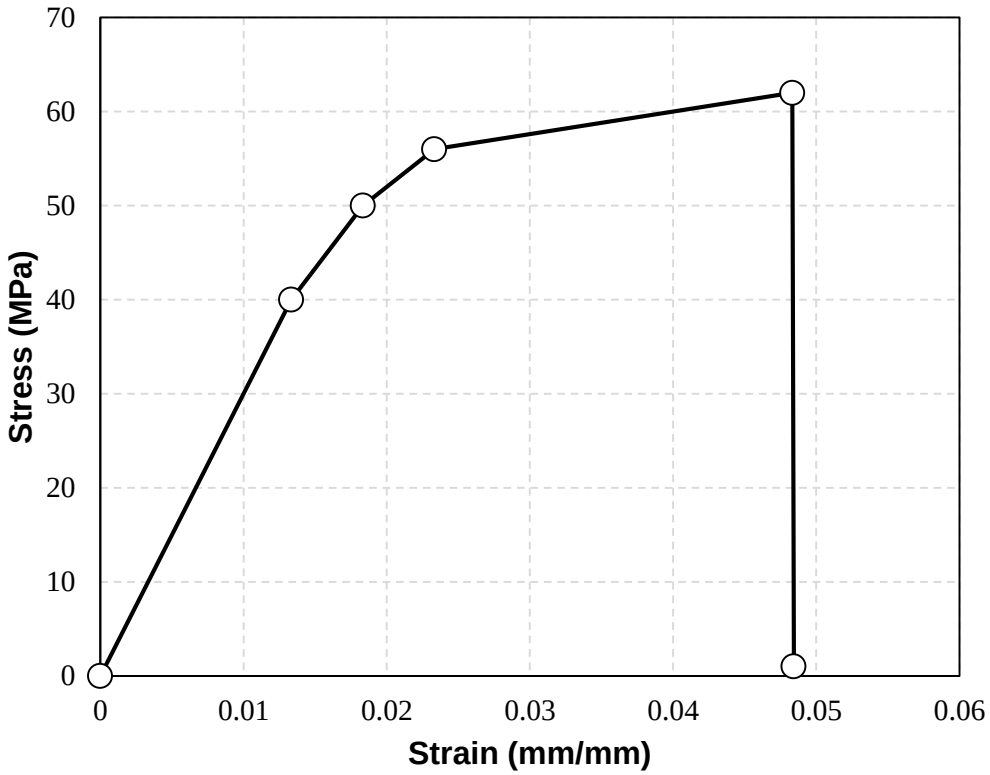

Figure 26. PLA constitutive stress-strain relationship used as input for the finite element models [11,65-67].

A simplification was made to model the post-tensioned fibers in specimen type F-I-F2 as equivalent axial compressive stresses on either face of the tension (bottom) flange. A conceptual schematic illustrating the application of the prestressing forces can be seen in **Figure 27**. Using this method, the use of elements representing reinforcing fibers, and the complexities resulting from fiber-matrix interfacial behavior, was avoided in this model. The prestressing force and equivalent compressive tractions that were input into each finite element model are presented in **Table 9**.

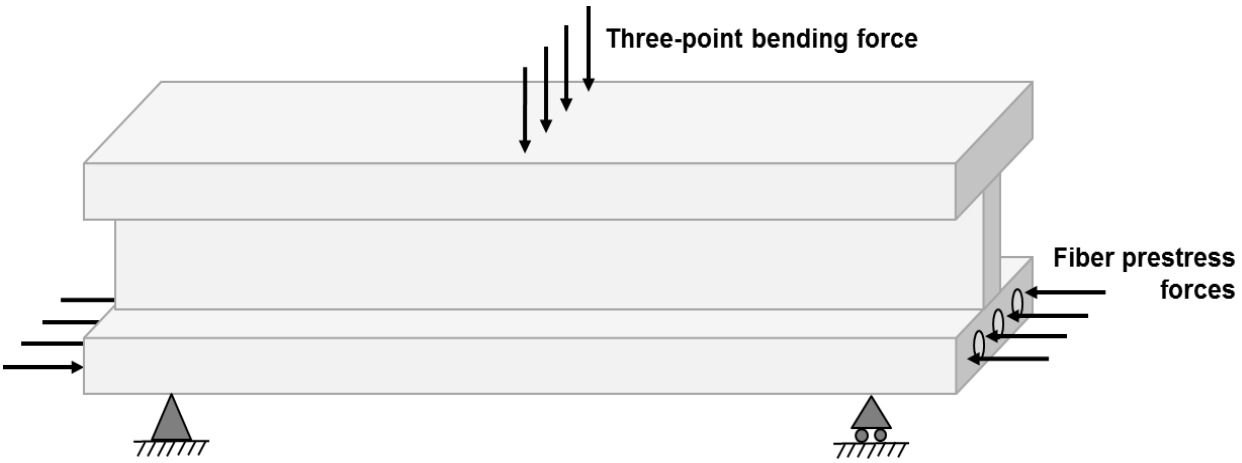

Figure 27. Schematic showing the concept of fiber prestressing forces providing initial moment counteracting applied three-point bending moment.

The 730 N prestressing force in the F-I-F2 model was divided by the cross-sectional area of the bottom flange of the ducted I-shape and applied on the flange as a compressive traction in the model, rather than creating fiber elements within the matrix voids and applying a prestressing force to them. **Figure 28** illustrates these compressive tractions applied in the model.

Table 9. Summary of prestressing forces used in each flexural specimen finite element model.

Specimen	Fiber prestressing force (N)	Equivalent model compressive traction (MPa)
F-I-U1	0	0
F-I-F2	730	13.6

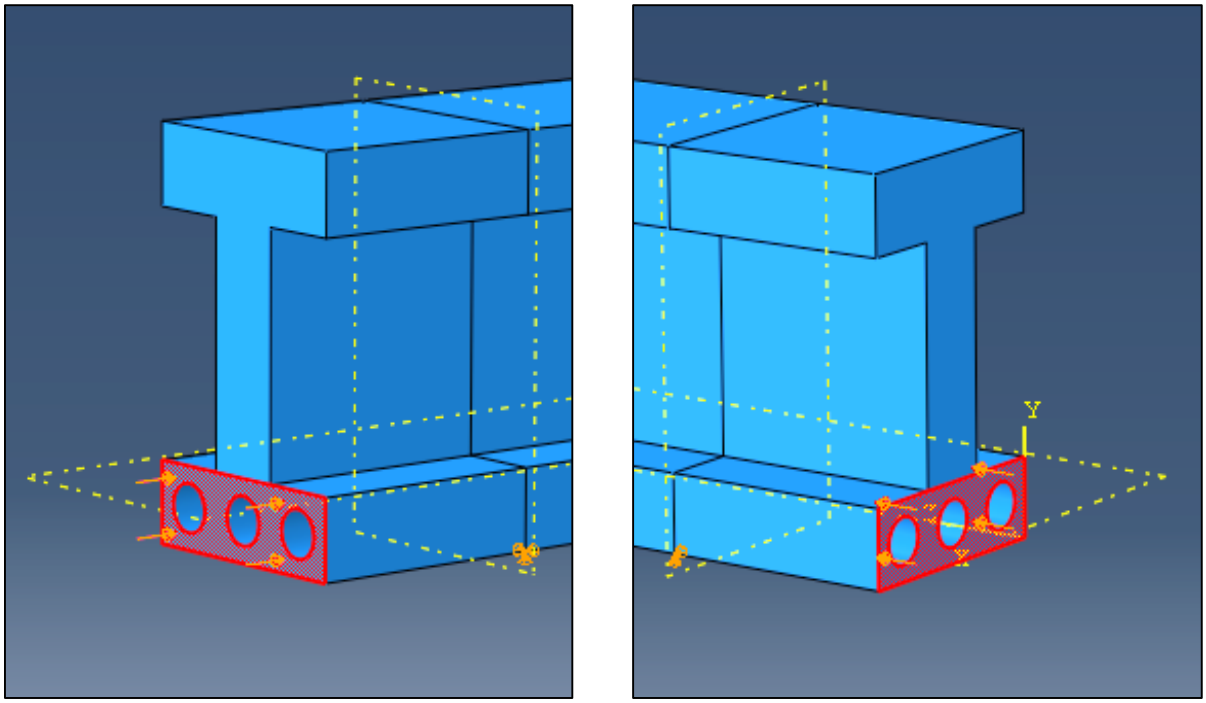

Figure 28. Prestressing force represented in finite element model as equivalent compressive tractions (orange arrows) on faces of bottom flange (red area).

A visualization of the resulting stresses in the flexural member and upward deflection (camber) after initial prestressing forces were applied is demonstrated in **Figure 29**. The stresses displayed in the figure occurred prior to the application of the three-point bending force in the model, and represent the highest compressive stresses as yellow and red coloration.

The three-point bending tests were simulated using static analysis, as well as constant displacement-controlled actuation to failure. The maximum applied midspan displacement was set to 8 mm and a 0.1-second step duration was used in each step. Internal stress, displacement, and reaction force data were extracted from the models after simulation completion. Flexural force-displacement curves were developed from these data for both specimen types, and compared in the following sections with the experimental force-displacement curves developed previously.

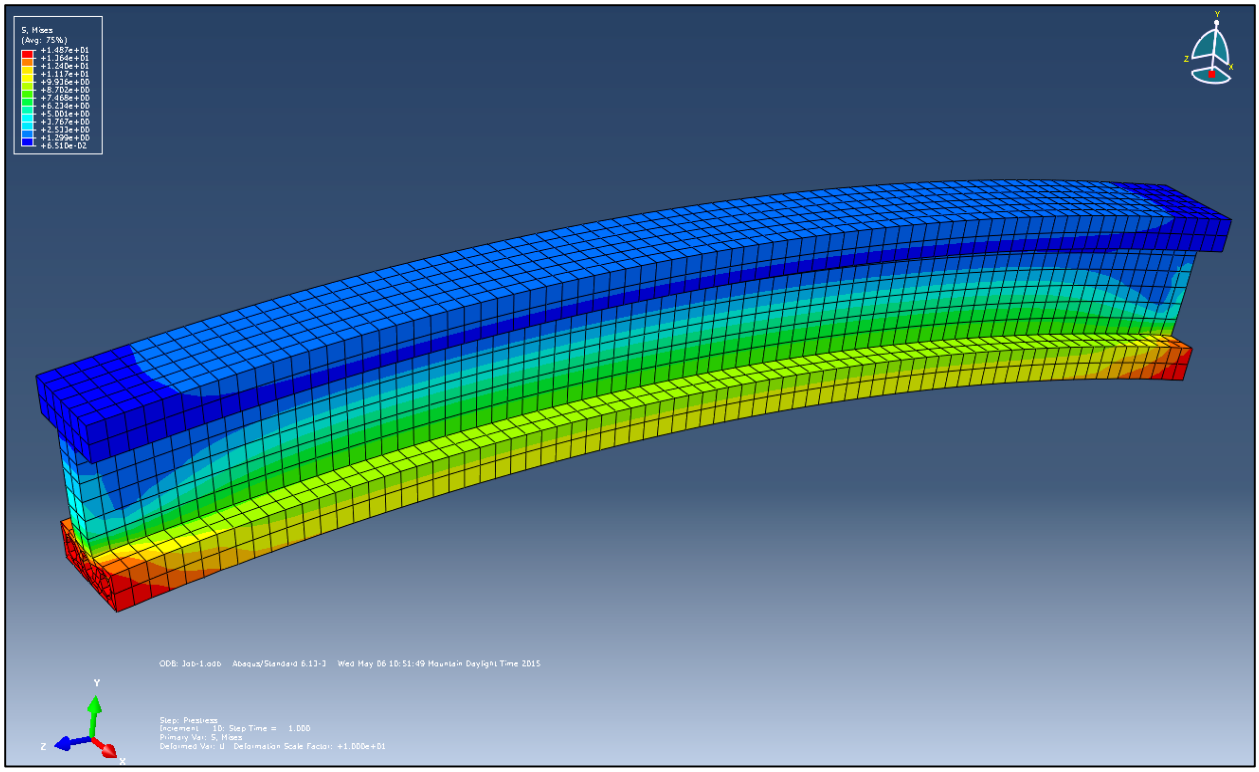

Figure 29. Visualization of Von Mises stress in finite element model of prestressed specimen (F-I-F2) after prestressing force applied (scale factor of 10).

4.2.2 Results

A visualization of the maximum Von Mises stresses experienced in the F-I-U1 specimen model during three-point bending is shown in **Figure 30**. The stress distribution for F-I-F2 specimen model was similar. As expected, maximum stress and plastification (indicated by the darkest red coloration) occurred at the top and bottom flanges of the flexural specimen during the three-point bending simulation.

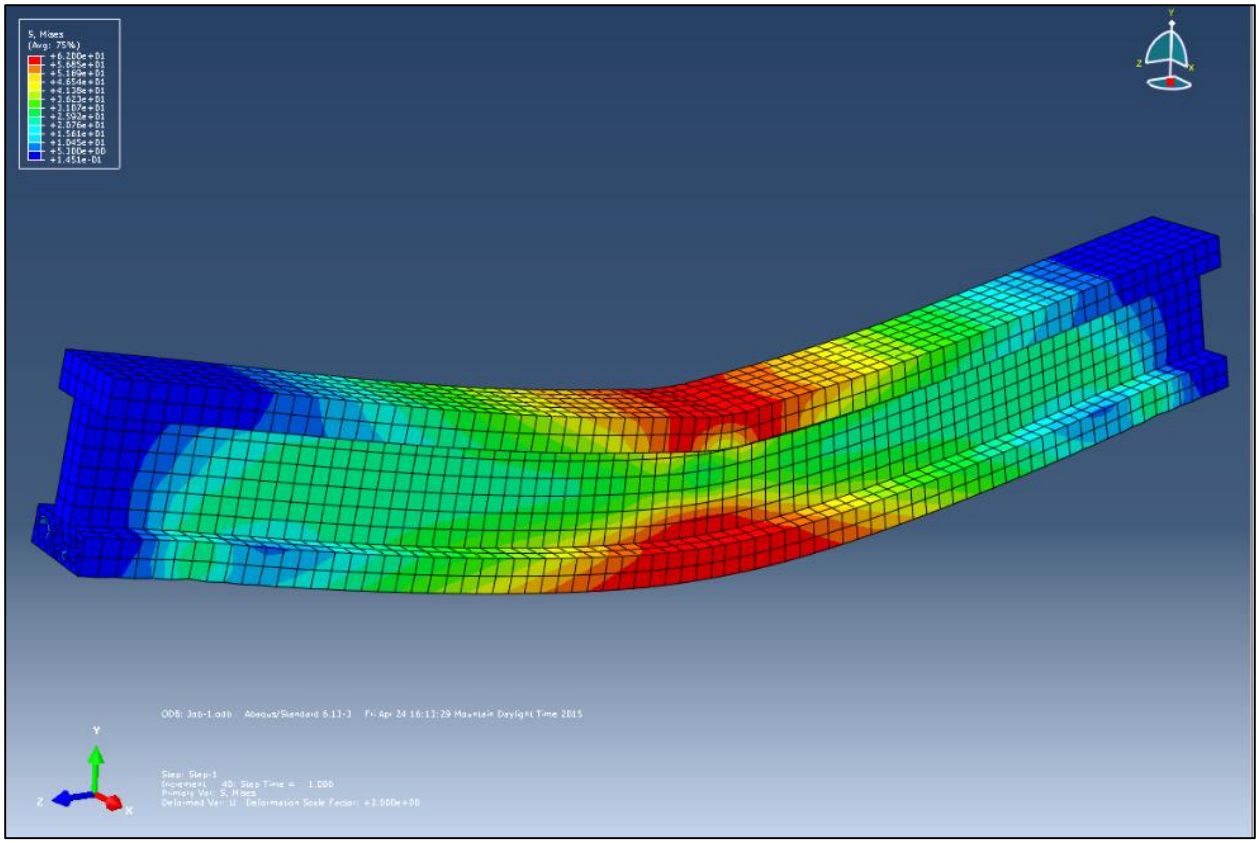

Figure 30. Visualization of Von Mises stress before failure in finite element model simulation of unreinforced ducted specimen (F-I-U1) three-point bending (scale factor of 5).

4.2.2.1 Comparison of unreinforced ducted and prestressed flax-reinforced finite element models

The flexural force-displacement behaviors obtained from the F-I-U1 and F-I-F2 specimen finite element model simulations are illustrated together in **Figure 31**. It is evident in the figure that the prestressed flexural specimen model exhibits higher flexural stiffness and strength, which is consistent with the experimental flexural specimen results and further substantiates the beneficial effect of prestressed fiber reinforcement on composite mechanical properties. However, the improvements in strength and stiffness due to prestressing observed from the model simulations were only 13% and 9%, respectively, compared to 21% and 15% from the

experimental tests. The discrepancies are likely attributable to the simplifications employed in the PLA constitutive relation and in the application of the fiber prestressing forces.

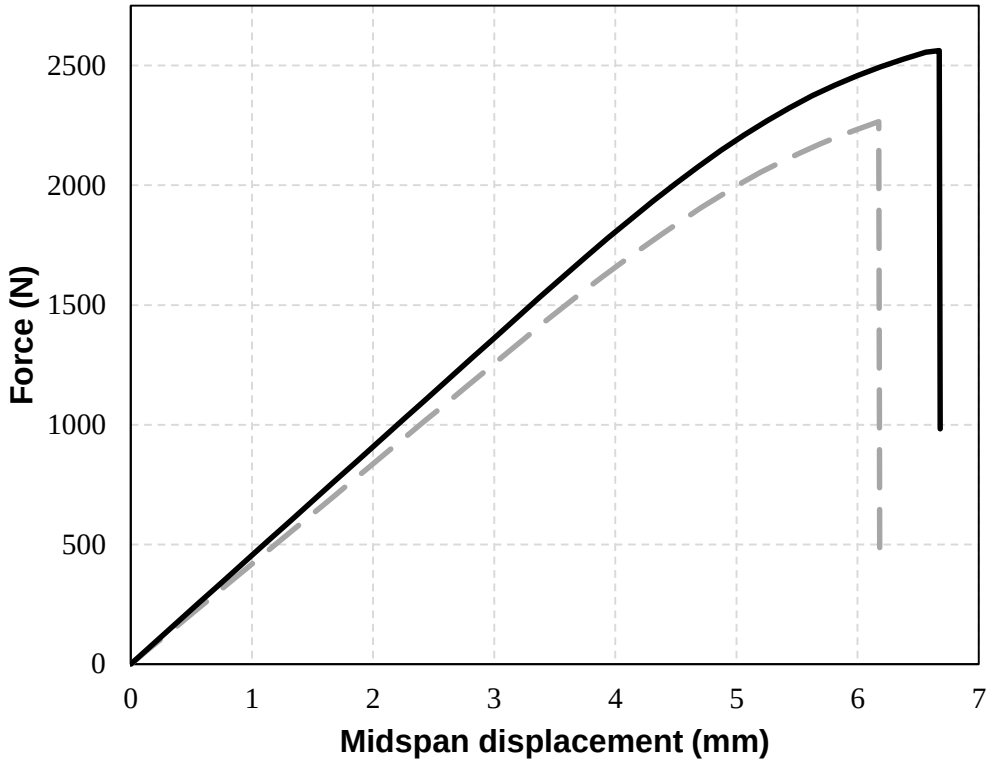

Figure 31. Finite element model simulated flexural force-displacement curves for F-I-U1 (— —) and F-I-F2 (—) specimens.

4.2.2.2 Unreinforced ducted flexural specimen experimental comparison

The force-displacement curve obtained from the unreinforced ducted specimen finite element model simulation is plotted along with the experimentally-obtained force-displacement curves in **Figure 32**. The figure clearly shows that the finite element model response curve falls within the experimental response curves, and is comparable in shape. More specifically, the strength, stiffness, and ultimate displacement calculated from the model simulation fall within 8%, 1%, and 5%, respectively, of the average of the corresponding experimentally-obtained properties.

The finite element model therefore appears to be an accurate representation of the F-I-U1 flexural specimen.

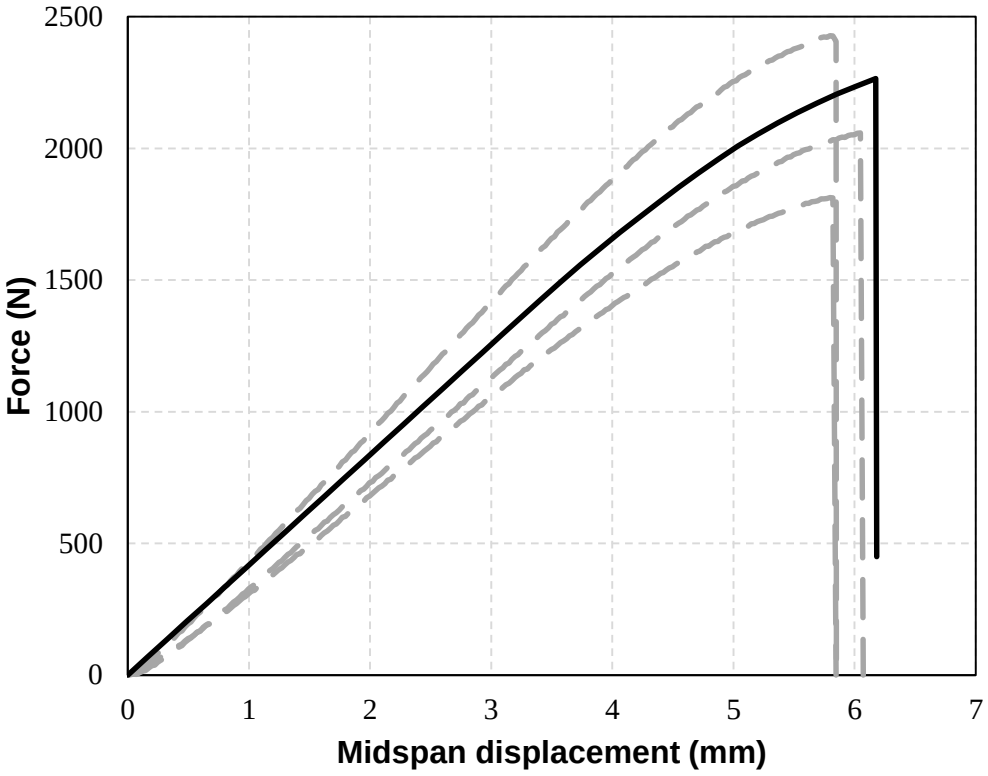

Figure 32. Experimental (— —) and finite element model simulated (—) flexural force-displacement curves for unreinforced ducted (F-I-U1) composite specimens.

4.2.2.3 Prestressed flax-reinforced flexural specimen experimental comparison

Similar to the F-I-U1 specimen, the force-displacement curve obtained from the prestressed flax-reinforced specimen finite element model simulation is plotted along with the experimentally-obtained force-displacement curves in **Figure 33**. Also similarly, the figure shows that the finite element model response curve falls acceptably within the experimental response curves, and is comparable in shape. Similar to the first model, the strength, stiffness, and ultimate displacement calculated from the second model simulation fall within 5%, 2%, and 1%, respectively, of the

average of the corresponding experimentally-obtained properties. The second finite element model also appears to be an accurate representation of the F-I-F2 flexural specimen.

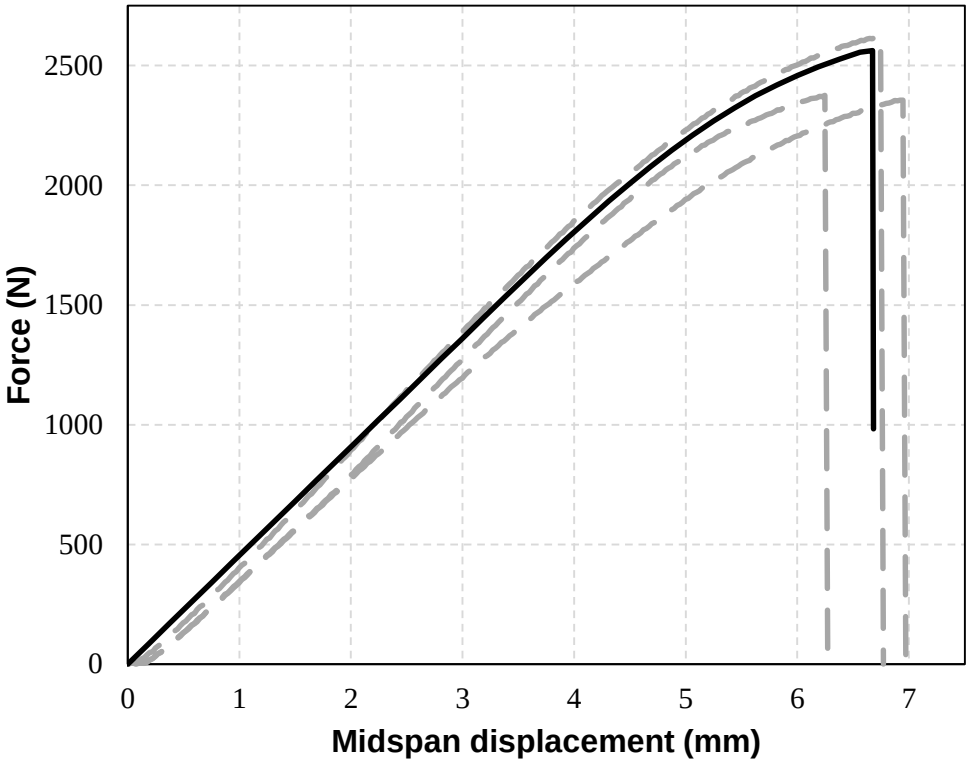

Figure 33. Experimental (— —) and finite element model simulated (—) flexural force-displacement curves for prestressed flax-reinforced (F-I-F2) composite specimens.

The two finite element models developed in this study accurately represented the two flexural composite specimens in mechanical response. Each finite element simulation exhibited similar mechanical response as its experimental counterpart, as evidenced by the model force-displacement curves falling reasonably within the experimentally-derived force-displacement curves. Additionally, the prestressed flexural specimen model showed improvement in flexural mechanical properties over the unreinforced specimen model, although slightly less improvement than observed in the experimentally-obtained mechanical properties. It is believed that this discrepancy likely stems from the simplifications used in the PLA constitutive relation and in

applying the prestressing forces to the models. In reality, the PLA matrix is not perfectly isotropic (differences exist between tensile and compressive properties, as shown in Chapter 2), and the omission of elements representing fiber reinforcement in the model possibly precludes realistic beneficial effects such as catenary action. Future modeling efforts should encompass these finer intricacies to improve model accuracy. However, even considering the simplifications and limitations of the finite element models presented herein, the results obtained are promising and further establish the feasibility of fiber reinforcement prestressing as a method to improve composite mechanical properties.

4.3 Predictive Analytical Equations

Analytical equations were developed from simple mechanics principles to predict strength- and stiffness-to-weight ratios for the prestressed tensile composite specimens that were presented and discussed in Chapter 2. The tensile mechanical property results obtained from the analytical equations are then compared to the results computed from the experimental data.

4.3.1 Definition of variables

The following input variables (**Table 10**) are used in the subsequent two sections (4.3.2 and 4.3.3) to derive the predictive analytical equations for tensile strength- and stiffness-to-weight ratios.

Table 10. Summary of input variables used in analytical equations.

Variable	Description
P	Applied tensile force
P_u	Ultimate composite tensile load

σ_m	Tensile stress in matrix
σ_{mu}	Ultimate tensile strength of matrix
A_m	Cross-sectional area of matrix
E_m	Tensile modulus of matrix
σ_f	Tensile stress in fibers
A_f	Area of fibers
d	Diameter of single fiber
E_f	Tensile modulus of fibers
n	Number of fibers in cross-section
W	Specimen weight
F_p	Initial fiber prestressing force
F_e	Equilibrium prestressing force

4.3.2 Tensile strength-to-weight ratio

Beginning with force equilibrium, the applied load, P, is expressed in terms of the force in the matrix, force in the fibers, and the equilibrium force resulting from the initial fiber prestressing force:

$$P = \sigma_m A_m + \sigma_f A_f + F_e \quad \text{Eq. 1}$$

With the assumption that matrix failure occurs first (which occurred in nearly every experimental test) and that both matrix and fiber experience equal strain at failure, the ultimate composite load, P_u, is expressed as:

$$\frac{\sigma_f}{E_f} = \frac{\sigma_{mu}}{E_m} \quad \text{Eq. 2}$$

$$A_f = \frac{n\pi d^2}{4} \quad \text{Eq. 3}$$

$$P_u = \sigma_{mu} A_m + \sigma_{mu} \frac{n\pi d^2}{4} \frac{E_f}{E_m} + F_e \quad \text{Eq. 4}$$

To determine the equilibrium force (F_e) resulting from the initial fiber prestressing force (F_p), first the initial strain in the fiber after initial prestressing, ε_{fi}, is calculated as:

$$\varepsilon_{fi} = \frac{4F_p}{n\pi d^2 E_f} \quad \text{Eq. 5}$$

from which the equilibrium force between the matrix and prestressed fibers after release (resulting from elastic shortening) can be determined as:

$$F_e = \frac{\varepsilon_{fi}}{\frac{1}{A_m E_m} + \frac{4}{n\pi d^2 E_f}} = \frac{\frac{4F_p}{n\pi d^2 E_f}}{\frac{1}{A_m E_m} + \frac{4}{n\pi d^2 E_f}} \quad \text{Eq. 6}$$

Substitution into the previous ultimate tensile load equation and simplifying yields:

$$P_u = \sigma_{mu} A_m + \sigma_{mu} \frac{n\pi d^2}{4} \frac{E_f}{E_m} + F_e = \sigma_{mu} A_m + \sigma_{mu} \frac{n\pi d^2}{4} \frac{E_f}{E_m} + \frac{\frac{4F_p}{n\pi d^2 E_f}}{\frac{1}{A_m E_m} + \frac{4}{n\pi d^2 E_f}} \quad \text{Eq. 7}$$

$$P_u = \sigma_{mu} \left(A_m + \frac{n\pi d^2}{4} \frac{E_f}{E_m} \right) + \frac{F_p}{1 + \frac{n\pi d^2}{4A_m} \frac{E_f}{E_m}} \quad \text{Eq. 8}$$

Normalizing the above ultimate tensile load equation by cross-sectional area and then by specimen weight gives the equations for composite tensile strength, σ_c, and composite tensile strength-to-weight ratio, σ'_t, respectively:

$$\sigma_c = \frac{P_u}{A_m} = \sigma_{mu} \left(1 + \frac{n\pi d^2}{4A_m} \frac{E_f}{E_m} \right) + \frac{F_p}{A_m + \frac{n\pi d^2}{4} \frac{E_f}{E_m}} \quad \text{Eq. 9}$$

$$\boldsymbol{\sigma'_t = \frac{\sigma_c}{W} = \frac{\sigma_{mu}}{W} \left(1 + \frac{n\pi d^2}{4A_m} \frac{E_f}{E_m} \right) + \frac{F_p}{W \left(A_m + \frac{n\pi d^2}{4} \frac{E_f}{E_m} \right)}} \quad \text{Eq. 10}$$

4.3.3 Tensile stiffness-to-weight ratio

Employing a rule-of-mixtures technique, the effective composite tensile modulus, E_{eff}, is given by:

$$E_{eff} = \frac{A_m E_m + A_f E_f}{A_m + A_f} \quad \text{Eq. 11}$$

$$E_{eff} = \frac{A_m E_m + \frac{n\pi d^2}{4} E_f}{A_m + \frac{n\pi d^2}{4}} \quad \text{Eq. 12}$$

Normalizing by specimen weight, the composite tensile stiffness-to-weight ratio, E'_t, is expressed as:

$$\boldsymbol{E'_t = \frac{E_{eff}}{W} = \frac{A_m E_m + \frac{n\pi d^2}{4} E_f}{W\left(A_m + \frac{n\pi d^2}{4}\right)}} \quad \text{Eq. 13}$$

4.3.4 Comparison of analytical to experimental results

Using the material properties, specimen dimensions, and prestressing forces presented in Chapter 2 as inputs, the two analytical equations were used to predict the tensile mechanical properties that were originally derived from experimental data. **Table 11** summarizes the analytical and experimental results for strength-to-weight and stiffness-to-weight ratios, and the percent differences between them. As indicated by the results table, all of the analytically-predicted tensile mechanical properties were greater than those that were computed from the experimental data. It is believed that the primary factors responsible for the discrepancies are (1) the analytical models only consider linear-elastic behavior, (2) the models assume complete rigidity in fiber anchorage, and (3) the models do not account for prestress losses and fiber relaxation. In reality, the matrix material does not exhibit a solely linear-elastic response, the anchorage system is not fully rigid,

and there is a strong likelihood that prestress losses occurred during experimental mechanical testing.

The jute-reinforced tensile specimen type was believed to have had the highest likelihood of experiencing prestress losses during experimental testing, and, as expected, it showed the highest strength discrepancy (26%) between analytical and experimental results. The three flax-reinforced specimen types remained below 20% difference. The stiffness-to-weight values indicated slightly lower differences between experimental and analytical, with all four specimens falling below 16%. Despite the discrepancies demonstrated between experimental and analytical values, the analytical models appear to provide fairly consistent overestimations of prestressed tensile specimen behavior, whose maximum difference of 26% may still be acceptable if anticipated.

Table 11. Comparison of experimentally- and analytically-obtained composite tensile specific mechanical properties.

Specimen Type	Strength-to-weight (MPa/g)		% Difference	Stiffness-to-weight (MPa/g)		% Difference
	Experimental	Analytical		Experimental	Analytical	
T-J1	3.74	4.72	26%	235	260	11%
T-F1	4.31	4.96	15%	273	316	16%
T-F2	4.55	5.27	16%	288	316	10%
T-F3	4.85	5.84	20%	298	338	13%

A technique to more accurately predict the tensile specific mechanical properties using equations 10 and 13 is the application of an adjustment factor to account for prestress losses, anchor flexibility, and other nonideal conditions. Calibrated to result in a percent error of 10% or less of the experimentally-obtained values, the adjustment factors that were used for strength-to-weight and stiffness-to-weight ratios were 0.87 and 0.95, respectively. Incorporating each corresponding adjustment factor into equations 10 and 13 produced adjusted analytical specific mechanical property values presented in **Table 12**, which are compared to the original experimental values. The adjusted analytical predictions of mechanical properties using appropriate adjustment factors result in differences of 10% or less — accuracy that is improved over the unadjusted analytical results and is considered adequate.

Table 12. Comparison of experimentally- and adjusted analytically-obtained composite tensile specific mechanical properties.

Specimen Type	Strength-to-weight (MPa/g)		% Difference	Stiffness-to-weight (MPa/g)		% Difference
	Experimental	Analytical		Experimental	Analytical	
T-J1	3.74	4.10	10%	235	247	5%
T-F1	4.31	4.31	0%	273	300	10%
T-F2	4.55	4.58	1%	288	300	4%
T-F3	4.85	5.08	5%	298	322	8%

CHAPTER 5
Conclusions

This study investigated the effect of initial fiber prestressing on the specific tensile and flexural properties of natural fiber-reinforced polylactic acid (PLA) composite materials. The effect of fiber type (e.g., jute, flax), matrix cross-sectional geometry, number of reinforcement strands, and level of initial fiber prestress on the strength-to-weight and stiffness-to-weight ratios of PLA matrices were examined herein.

Experimental results confirm that utilizing additive manufacturing (3D printing) to produce more efficient structural shapes improves the specific tensile and flexural mechanical properties of PLA composites and that these properties are further improved via initial fiber post-tensioning. Given the superior tensile properties of flax fibers compared to jute fibers, the flax-reinforced members exhibited the most notable improvement in specific mechanical properties. The data suggest increases of 116% and 32% in specific strength and 62% and 29% in specific stiffness in tension and flexure, respectively, compared to unreinforced PLA matrices. The improvements in strength due to fiber prestressing, which are sometimes not observed in analogous prestressed concrete applications, are attributable to the induction of higher degrees of compressive forces in the PLA matrices, requiring higher applied loads to initiate the governing tensile failure of the matrices. To further validate the experimental results, flexural specimen finite element model simulation results exhibited reasonable agreement with the experimental results, also showing that flexural mechanical properties can be improved with the addition of post-tensioned reinforcing fibers. Analytical predictive equations also produced tensile mechanical property predictions that, although consistently overestimated, aligned reasonably with the experimental tensile results, especially after applying adjustment factors.

Despite existing challenges associated with prestressed NFCs (e.g., fiber variability, anchorage systems, biopolymer economics), the results presented in this study suggest that prestressing natural fibers is a promising new paradigm for advancing the field of natural fiber composite science and engineering.

5.1 Advantages, Challenges, and Future Opportunities

The results obtained from the mechanical tests indicate that fiber prestressing is a viable technique that can be employed to more fully utilize the inherently high stiffness and strength of natural fibers in the design and fabrication of high-performance NFCs. Composites with higher specific properties indicate a more efficient use of material constituents, which translates to reductions in overall material quantities. Minimizing material quantities (and minimizing waste due to the use of additive manufacturing) has obvious economic and environmental implications.

Despite the positive results obtained in this study, several challenges exist for obtaining consistent behavior and mechanical property results for prestressed NFCs. These challenges are evident in the high variability of the material property results presented herein. For example, the prestressed tensile composite specimens exhibited particularly high variability in specific mechanical properties. This variability can be attributed to (1) variation in fiber properties, (2) inconsistency in prestressed fiber anchorage and resulting prestress losses, and (3) variability in 3D print quality. Variation in fiber properties is often cited as a limitation of NFCs. However, the variability can be reduced by using fiber yarns and bundles and by conducting initial fiber tests prior to prestressed-fiber applications. Future advances in plant genetics will also contribute consistency in industrial plant products. More advanced characterization (e.g., scanning electron microscopy) of the fiber cross-sectional properties should be employed in future studies to more

accurately portray fiber strength and stiffness, such as performed in other natural fiber studies [30,31,37]. Subsequent investigations should also consider the effectiveness of different prestressing anchorage techniques. Relatedly, research is needed on expected loss in prestressing due to different anchorage systems and techniques. Refinement of anchorage systems would likely result in less prestress loss in the fibers and, consequently, higher improvements in composite mechanical properties. Finally, variability in 3D printing quality will likely improve along with the resolution and consistency of 3D printing technology.

In addition, a number of scientific and economic challenges exist before biobased NFCs become viable alternatives to synthetic, petroleum-based composites. Despite proven environmental benefits of composites from biorenewable resources, fully biobased composites not only exhibit low specific mechanical properties (as addressed herein), but also demonstrate poor moisture resistance [68-70], susceptibility to long-term viscoelastic deformation under sustained loads (creep) [71,72], and sensitivity to high temperatures [73]. Creep was likely not a significant factor in this study due to the relatively brief time frames considered, but would be an expected issue in in-service construction applications, which is currently receiving attention in the NFC research community [67,73-75]. Another challenge requiring attention that is also related to the long-term performance of prestressed NFCs is the gradual relaxation of the prestressing fibers, which contributes to the decay of mechanical performance [3].

Furthermore, biopolymers and bioplastics currently face economic constraints. While significant research is currently being conducted on improving the hygrophobicity of natural fibers through physical and chemical fiber treatments [33] and creep deformation [73-76], biopolymer matrices (e.g., PLA, PHB) are costly to manufacture compared to many synthetic polymers. It is believed, however, that this cost will decrease with increasing demand [77]. National policies and

green building programs are important factors that contribute to the future bioplastics market. For example, the International Organization for Standards (ISO), green building certification programs (e.g., United States Green Building Council), and the introduction of Environmental Product Declarations (EPD) — certified documents that promote transparency in materials manufacturing — are further prompting increased demands for building and construction materials from biorenewable resources.

Opportunities exist to leverage this foundational work in developing novel classes of high-performance natural-fiber composites. While this study investigated the mechanical performance of two natural fibers, namely jute and flax, one biopolymer (PLA), and two geometric arrangements, the proposed fiber prestressing technique is potentially viable for other geometries, natural fibers (e.g., silk, hemp, kenaf, abaca), and polymer matrices. Further experimental and theoretical research is needed, however, to evaluate the performance of natural fibers in combination with other polymer matrix systems. More detailed and complex finite element models, as well as analytical equations, would allow for not only more accurate predictions, but more widely applicable (i.e., other biopolymers and natural fibers) predictions. After more such research is performed, the further refinement of applied mathematical models for use in engineering design with prestressed biocomposite materials would be a valuable next step in implementing them into practical construction applications. These future efforts offer much promise in establishing the fundamental science and engineering of prestressed NFCs.

BIBLIOGRAPHY

1. Bakis, C., Bank, L., Brown, V., Cosenza, E., Davalos, J., Lesko, J., Machida, A., Rizkalla, S., Triantafillou, T. (2002). "Fiber-reinforced polymer composites for construction—state-of-the-art review." *Journal of Composites for Construction*, 6, p. 73.
2. Dittenber, D.B., GangaRao, H.V.S. (2012). "Critical review of recent publications on use of natural composites in infrastructure." *Composites: Part A*, 43, pp. 1419-1429.
3. Zou, P.X.W. (2003). "Long-term properties and transfer length of fiber-reinforced polymers." *Journal of Composites for Construction*, 7(1), pp. 10-19.
4. Sandler, K. (2003). "Analyzing what's recyclable in C&D debris." *BioCycle*, pp. 51-54.
5. Hess, K.M., Srubar III, W.V. (2014). "Mechanical characterization of gelatin-based natural fiber composites for construction." *Journal of Renewable Materials*.
6. Michel, A.T. (2012). *Characterization and modeling of biobased composites and structural insulated panels*. (Doctoral dissertation).
7. John, M.J., Thomas, S. (2008). "Biofibres and biocomposites." *Carbohydrate Polymers*, 71, pp. 343-364.
8. Sheth, M., Kumar, R.A., Dave, V., Gross, R.A., McCarthy, S.P. (1996). "Biodegradable polymer blends of poly(lactic acid) and poly(ethylene glycol)." *Journal of Applied Polymer Science*, 66(8), pp. 1495-1505.
9. Christian, S., Billington, S. (2011). "Mechanical response of PHB- and cellulose acetate natural fiber-reinforced composites for construction applications." *Composites: Part B*, 42(7), pp. 1920-1928.

10. Hu, R., Lim, J. (2007). "Fabrication and mechanical properties of completely biodegradable hemp fiber reinforced polylactic acid composites." *Journal of Composite Materials*, 41(13), pp. 1655-1669.
11. Van de Velde, K., Kiekens, P. (2002). "Biopolymers: overview of several properties and consequences on their applications," *Polymers Testing*, 21, pp. 433-442.
12. Faruk, O., Bledzki, A.K., Fink, H., Sain, M. (2012). "Biocomposites reinforced with natural fibers: 2000-2010." *Progress in Polymer Science*, 37, pp. 1552-1596.
13. Kalia, S., Kaith, B.S., Kaur, I. (2009). "Pretreatments of natural fibers and their applications as reinforcing material in polymer composites—a review." *Polymer Engineering and Science*, 49, pp.1253-1272.
14. Oksman, K., Skrifvars, M., Selin, J.-F. (2003). "Natural fibers as reinforcement in polylactic acid (PLA) composites." *Composites Science and Technology*, 63, pp. 1317-1324.
15. Wambua, P., Ivens, J., Verpoest, I. (2003). "Natural fibers: can they replace glass in fibre reinforced plastics?" *Composites Science and Technology*, 63, pp. 1259-1264.
16. Holbery, J., Houston, D. (2006). "Natural fiber-reinforced polymer composites in automotive applications." *JOM*, 58(11), pp. 80-86.
17. Mohanty, A.K., M. Misra, Drzal, L.T. (2002). "Sustainable bio-composites from renewable resources: opportunities and challenges in the green materials world." *Journal of Polymers and the Environment*, 10(1), pp. 19-26.
18. Pietrini, M., Roes, L., Patel, M.K., Cheillini, E. (2007). "Comparative Life Cycle Studies on Poly(3-hydroxybutyrate)-Based Composites as Potential Replacement for Conventional Petrochemical Plastics." *Biomacromolecules*, 8(7), pp. 2210-2218.

19. Baillie, C., Ed. (2004). *Green Composites: Polymer Composites and the Environment*, CRC Press, Cambridge, UK.
20. Thomas, S., Pothan, L.A. (2009). *Natural Fibre Reinforced Polymer Composites: From Macro to Nanoscale*, Old City, Philadelphia, USA.
21. Bodros, E., Pillin, I., Montrelay, N., Baley, C. (2007). "Could Biopolymers Reinforced by Randomly Scattered Flax Fibre be Used in Structural Applications?" *Composites Science and Technology*, 67(3-4), pp. 462-470.
22. Alvarez, V.A., Fraga, A.N., Vazquez, A. (2004), "Effects of the Moisture and Fiber Content on the Mechanical Properties of Biodegradable Polymer-Sisal Fiber Biocomposites." *Journal of Applied Polymer Science*, 91, pp. 4007-4016.
23. Srubar III, W.V., Pilla, S., Wright, Z.C., Ryan, C.A., Greene, J.P., Frank, C.W., Billington, S.L. (2012). "Mechanisms and Impact of Fiber-Matrix Compatibilization Techniques on the Material Characterization of PHBV/Oak Wood Flour Engineered Biobased Composites." *Composites Science and Technology*; 72(6), pp. 708-15.
24. Lackey, E., Vaughan, J.G., Inamdar, K., Hancock, B. (2004). "Statistical Characterization of Pultruded Composites with Natural Fiber Reinforcements," in *COMPOSITES 2004: American Composites Manufacturers Association*: Tampa, Florida.
25. Bledzki, A.K., Jaszkiewicz, A. (2010). "Mechanical performance of biocomposites based on PLA and PHBV reinforced with natural fibres – A comparative study to PP." *Comp Sci TechI*, 70(12), pp. 1687-1696.
26. Plackett, D., Andersen, T., Pedersenc, W., Nielsen, L. (2003). "Biodegradable composites based on l-polylactide and jute fibres." *Comp Sci Tech*, 63(9), pp. 1287-1296.

27. Singh, B., Gupta, M. (2005). "Natural Fiber Composites for Building Application," in *Natural Fibers, Biopolymers, and Biocomposites*. Mohanty, A.K., Misra, M., and L.T. Drzal, Eds. CRC Press, Taylor & Francis Group: Boca Raton, FL, pp. 261-290.
28. Billington, S.L., Srubar III, W.V., Miller, S.A., Michel, A.T. (2013). "Renewable Biobased Composites for Civil Engineering Applications." in *Sustainable Composites and Advanced Materials*. Netravali, A. and C. Pastore, Eds. DESTech: Lancaster, PA, pp. 313-336.
29. Srubar III, W.V., Billington, S.L. (2013). "A Micromechanical Model for Moisture-Induced Deterioration in Fully Biorenewable Wood-Plastic Composites." *Composites Part A: Applied Science and Manufacturing*, 50, pp. 81-92.
30. Symington, M., Banks, W.N., West, O.D., Pethrick, R.A. (2009). "Tensile Testing of Cellulose Based Natural Fibers for Structural Composite Applications." *Journal of Composite Materials*, 43(9), pp. 1083-1108.
31. Cheung, H.-Y., Lau, K.-T., Ho, M.-P., Mosallam, A. (2009). "Study on the Mechanical Properties of Different Silkworm Silk Fibers." *Journal of Composite Materials*, 43(22), pp. 2521-31.
32. Avella, M., Martuscelli, E., Raimo, M. (2000). "Review Properties of blends and composites based on poly (3-hydroxy) butyrate (PHB) and poly (3-hydroxybutyrate-hydroxyvalerate)(PHBV) copolymers." *Journal of Materials Science*, 35(3), pp. 523-545.
33. George, J., Sreekala, M.S., Thomas, S. (2001) "A review on interface modification and characterization of natural fiber reinforced plastic composites." *Polymer Engineering & Science*, 41(9), pp. 1471-1485.
34. Sydenstricker, T.H.D., Mochnaz, S., Amico, S.C. (2003). "Pull-out and other evaluations in sisal-reinforced polyester biocomposites." *Polymer Testing*, 22, pp. 375-380.

35. Graupner, N., Herrmann, A.S., Mussig, J. (2009). "Natural and man-made cellulose fibre-reinforced poly(lactic acid) (PLA) composites: and overview about mechanical characteristics and application areas." *Composites: Part A,* 40, pp. 810-821.
36. Abilash, N., Sivapragash, M. (2013). "Environmental benefits of eco-friendly natural fiber reinforced polymeric composite materials." *International Journal of Application or Innovation in Engineering & Management,* 2(1), pp. 53-59.
37. Silva, F., Chawla, N., Filho, R.D. (2008). "Tensile behavior of high performance natural (sisal) fibers." *Composites Science and Technology,* 68, pp. 3438-3443.
38. Li, Y., Mai, Y.-W., Ye, L. (2000). "Sisal fibre and its composites: a review of recent developments." *Composites Science and Technology,* 60, pp. 2037-2055.
39. Corbiere-Nicollier, T., Laban, B.G., Lundquist, L., Leterrier, Y., Manson, J.-A.E., Jolliet, O. (2001). "Life cycle assessment of biofibres replacing glass fibres as reinforcement in plastics." *Resources, Conservation, and Recycling,* 33, pp. 267-287.
40. Garrain, D., Vidal, R., Martinez, P., Franco, V., Gonzalez, R. (2007). "How 'green' are biopolymers?" *International Conference on Engineering Design.*
41. Joshi, S.V., Drzal, L.T., Mohanty, A.K., Arora, S. (2003). "Are natural fiber composites environmentally superior to glass fiber reinforced composites?" *Composites: Part A,* 35, pp. 371-376.
42. Herrera-Franco, P.J., Valadez-Gonzalez, A. (2004). "Mechanical properties of continuous natural fibre-reinforced polymer composites." *Composites: Part A,* 35, pp. 339-345.
43. Ku, H., Wang, H., Pattarachaiyakoop, N., Trada, M. (2011). "A review on the tensile properties of natural fiber reinforced polymer composites." *Composites: Part B,* 42, pp. 856-873.

44. Rong, M.Z., Zhang, M.Q., Liu, Y., Yang, G.C., Zeng, H.M. (2001). "The effect of fiber treatment on the mechanical properties of unidirectional sisal-reinforced epoxy composites." *Composites Science and Technology*, 61, pp. 1437-1447.
45. Burgueno, R., Quagliata, M.J., Mohanty, A.K., Mehta, G., Drzal, L.T., Misra, M. (2004). "Load-bearing natural fiber composite cellular beams and panels." *Composites: Part A*, 35, pp. 645-656.
46. Burgueno, R., Quagliata, M.J., Mohanty, A.K., Mehta, G., Drzal, L.T., Misra, M. (2005). "Hybrid biofiber-based composites for structural cellular plates." *Composites: Part A*, 36, pp. 581-593.
47. Lim, L.T., Auras, R., Rubino, M. (2008). "Processing technologies for poly(lactic acid)." *Progress in Polymer Science*, 33(8), pp. 820-852.
48. Liao, Q., Tsui, A., Billington, S., Frank, C. (2012). "Extruded foams from microbial poly (3-hydroxybutyrate-co-3-hydroxyvalerate) and its blends with cellulose acetate butyrate." *Polymer Engineering & Science*, 52(7), pp. 1495-1508.
49. Lee, S. T., Kareko, L., Jun, J. (2008). "Study of thermoplastic PLA foam extrusion." *Journal of cellular plastics*, 44(4), 293-305.
50. Srubar III, W.V., Billington, S.L. (2011). "Engineered biobased composites for construction: material development, multiscale modeling, and long-term durability." *Structures Congress*.
51. Dhakal, H.N., Zhang, Z.Y., Richardson, M.O.W. (2007) "Effect of water absorption on the mechanical properties of hemp fibre reinforced unsaturated polyester composites." *Composites Science and Technology*, 67, pp. 1674-1683.

52. Mathew, A.P., Oksman, K., Sain, M. (2005). "The effect of morphology and chemical characteristics of cellulose reinforcements on the crystallinity of polylactic acid." *Journal of Applied Polymer Science,* 101(1), pp. 300-310.
53. Huda, M.S., Drzal, L.T., Misra, M. (2005). "A study on biocomposites from recycled newspaper fiber and poly(lactic acid)." *Industrial & Engineering Chemistry Research,* 44, pp. 5593-5601.
54. Pilla, S., Gong, S., O'Neill, E., Yang, L., Rowell, R.M. (2008). "Polylactide-recycled wood fiber composites." *Journal of Applied Polymer Science,* 111, pp. 37-47.
55. Naaman, A.E. (2012). *Prestressed Concrete Analysis and Design:* Techno Press 3000, Ann Arbor, MI.
56. Benaim, R. (2008). *The Design of Prestressed Concrete Bridges:* Taylor & Francis, New York, NY.
57. Motahhari, S., Cameron, J. (1999). "Fibre prestressed composites: improvement of flexural properties through fibre prestressing." *Journal of reinforced plastics and composites*, 18(3), pp. 279-288.
58. Fazal, A., Fancey, K.S. (2014). "UHMWPE fibre-based composites: Prestress-induced enhancement of impact properties." *Composites Part B: Engineering*, 66, pp. 1-6.
59. Fazal, A., Fancey, K.S. (2014). "Performance enhancement of nylon/kevlar fiber composites through viscoelastically generated pre-stress." *Polymer Composites*, 35(5), pp. 931-938.
60. Fancey, K. (2000). "The Effects of fibre pre-stressing on the impact performance of composite laminates." *Journal of Reinforced Plastics and Composites,* 19(15), pp. 1251-66.

61. El-Hacha, R., Wight, R.G., Green, M.F. (2001). "Prestressed fibre-reinforced polymer laminates for strengthening structures." *Progress in Structural Engineering Materials*, 3; pp. 111-21.

62. Erki, M.A., Rizkalla, S.H. (1993). "FRP reinforcement for concrete structures." *Concrete International*, pp. 48-53.

63. Schlichting, L.H., de Andrada, M.A., Vieira, L.C., Barra, G.M., Magne, P. (2010). "Composite resin reinforced with pre-tensioned glass fibers: Influence of prestressing on flexural properties." *Dental Materials*, 26(2), pp. 118-25.

64. Eichhorn, S.J., Baillie, C.A., Zafeiropoulos, N. (2001). "Review: Current international research into cellulosic fibres and composites." *Journal of Materials Science,* 36, pp. 2107-2131.

65. Iwatake, A., Nogi, M., Yano, H. (2008). "Cellulose nanofiber-reinforced polylactic acid." *Composites Science and Technology*, 68, pp. 2103-2106.

66. Jonoobi, M., Harun, J., Mathew, A.P., Oksman, K. (2010). "Mechanical properties of cellulose nanofiber (CNF) reinforced polylactic acid (PLA) prepared by twin screw extrusion." *Composites Science and Technology,* 70, pp. 1742-1747.

67. Suryanegara, L., Nakagaito, A.N., Yano, H. (2010). "Thermo-mechanical properties of microfibrillated cellulose-reinforced partially crystallized PLA composites." *Cellulose,* 17(4), pp. 771-778.

68. Espert, A., F. Vilaplana, Karlsson, S. (2004). "Comparison of water absorption in natural cellulosic fibres from wood and one-year crops in polypropylene composites and its influence on their mechanical properties." *Composites. Part A, Applied science and manufacturing*, 35(11), pp. 1267-1276.

69. Almgren, K.M., Gamstedt, E.K., Berthold, F., Lindstrom, M. (2009). "Moisture uptake and hygroexpansion of wood fiber composite materials with polylactide and polypropylene matrix materials." *Polymer Composites*, 30(12), pp. 1809-1816.
70. Wang, W., Sain, M., Cooper, P.A. (2006). "Study of moisture absorption in natural fiber plastic composites." *Composites Science and Technology*, 66(3-4), pp. 379-386.
71. Alvarez, V.A., Kenny, J.M., Vázquez, A. (2004). "Creep behavior of biocomposites based on sisal fiber reinforced cellulose derivatives/starch blends." *Polymer Composites*, 25(3), pp. 280-288.
72. Cyras, V., Martucci, J.F., Iannace, S., Vazquez, A. (2002). "Influence of the Fiber Content and the Processing Conditions on the Flexural Creep Behavior of Sisal-PCL-Starch Composites." *Journal of Thermoplastic Composite Materials*, 15(3), pp. 253-265.
73. Tajvidi, M., Motie, N., Rassam, G., Falk, R., Felton, C. (2010). "Mechanical performance of hemp fiber polypropylene composites at different operating temperatures." *Journal of Reinforced Plastics and Composites,* 29(5), pp. 664-674.
74. Hamel, S.E., Hermanson, J.C., Cramer, S.M. (2011). "Mechanical and time-dependent behavior of wood-plastic composites subjected to tension and compression." *Journal of Thermoplastic Composite Materials,* pp. 1-20.
75. Hamel, S.E., Hermanson, J.C., Cramer, S.M. (2015). "Mechanical and time-dependent behavior of wood-plastic composites subjected to bending." *Journal of Thermoplastic Composite Materials,* 28(5), pp. 630-642.
76. Wong, S., Shanks, R., Hodzic, A. (2004). "Interfacial improvements in poly (3-hydroxybutyrate)-flax fibre composites with hydrogen bonding additives." *Composites Science and Technology,* 64(9), pp. 1321-1330.

77. Chanprateep, S. (2010). “Current trends in biodegradable polyhydroxyalkanoates.” *Journal of bioscience and bioengineering*, 110(6), pp. 621-632.

78. Gilding, D.K., Reed, A.M. (1979). “Biodegradable polymers for use in surgery—polyglycolic/poly(lactic acid) homo- and copolymers: 1.” *Polymer*, 20(12), pp.1459-1464.

79. Lou, T.-J., Xiang, Y.-Q. (2006). “Finite element modeling of concrete beams prestressed with external tendons.” *Engineering Structures*, 28, pp. 1919-1926.

80. Ozcan, D.M., Bayraktar, A., Sahin, A., Haktanir, T., Turker, T. (2009). “Experimental and finite element analysis on the steel fiber-reinforced concrete (SFRC) beams ultimate behavior.” *Construction and Building Materials*, 23, pp. 1064-1077.

81. Garlotta, D. (2001). “A literature review of poly(lactic acid).” *Journal of Polymers and the Environment*, 9(2), pp. 63-84.

APPENDIX A

Tensile Data

A.1 Fiber Tensile Test Data

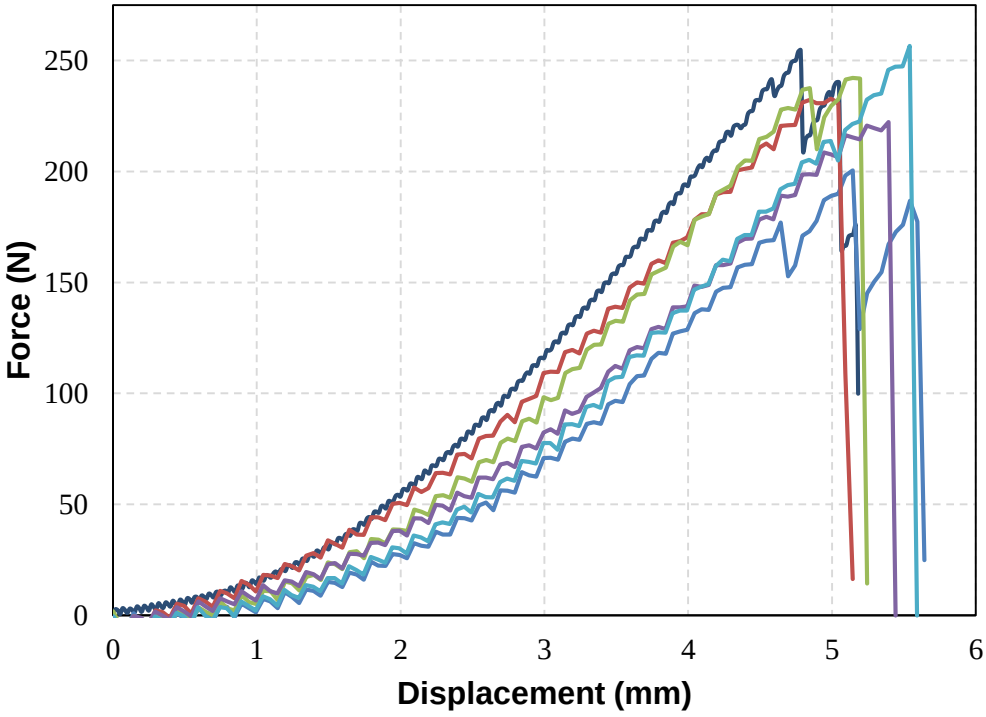

Figure 34. Experimental tensile force-displacement data for jute fiber samples.

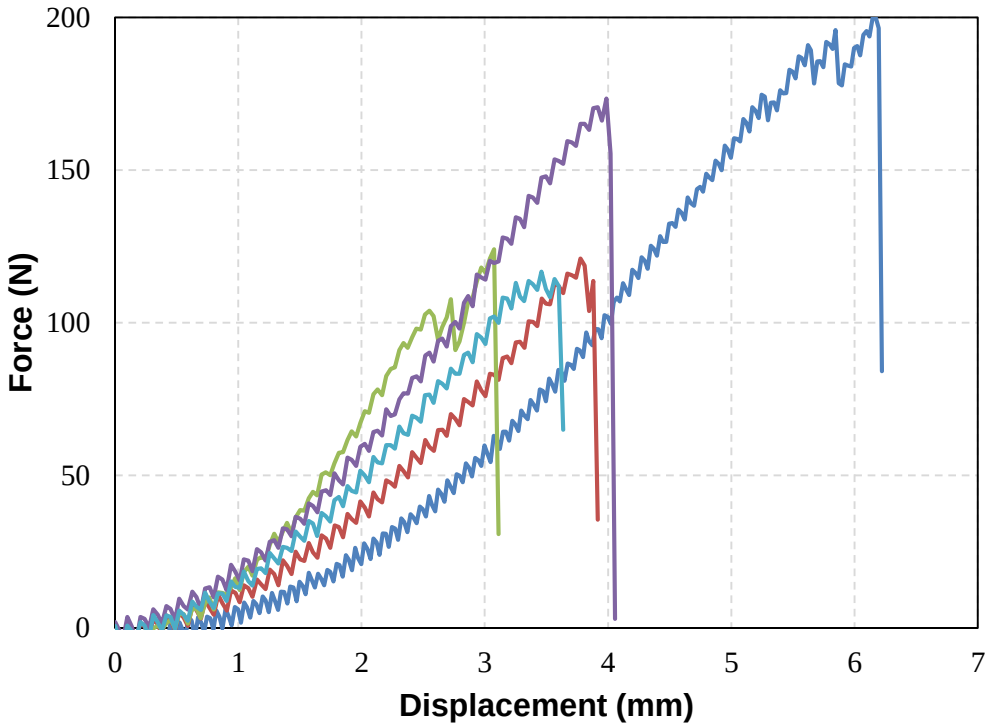

Figure 35. Experimental tensile force-displacement data for flax fiber samples.

A.2 PLA Compressive Test Data

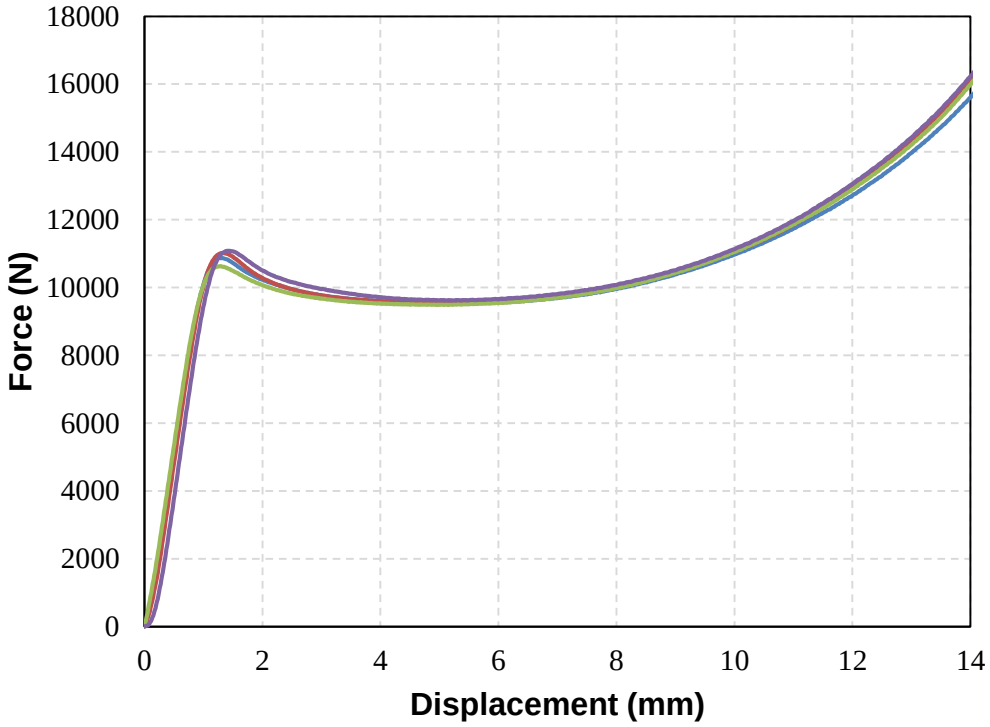

Figure 36. Experimental compressive force-displacement data for solid PLA samples.

A.3 Composite Specimen Tensile Test Data

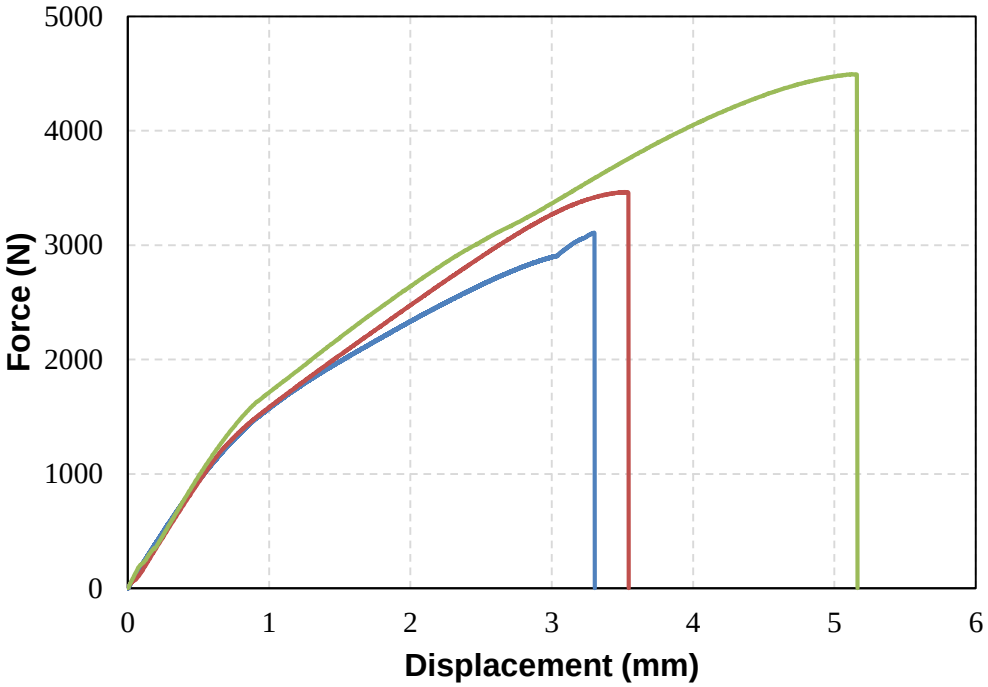

Figure 37. Experimental tensile force-displacement data for specimen type T-S1.

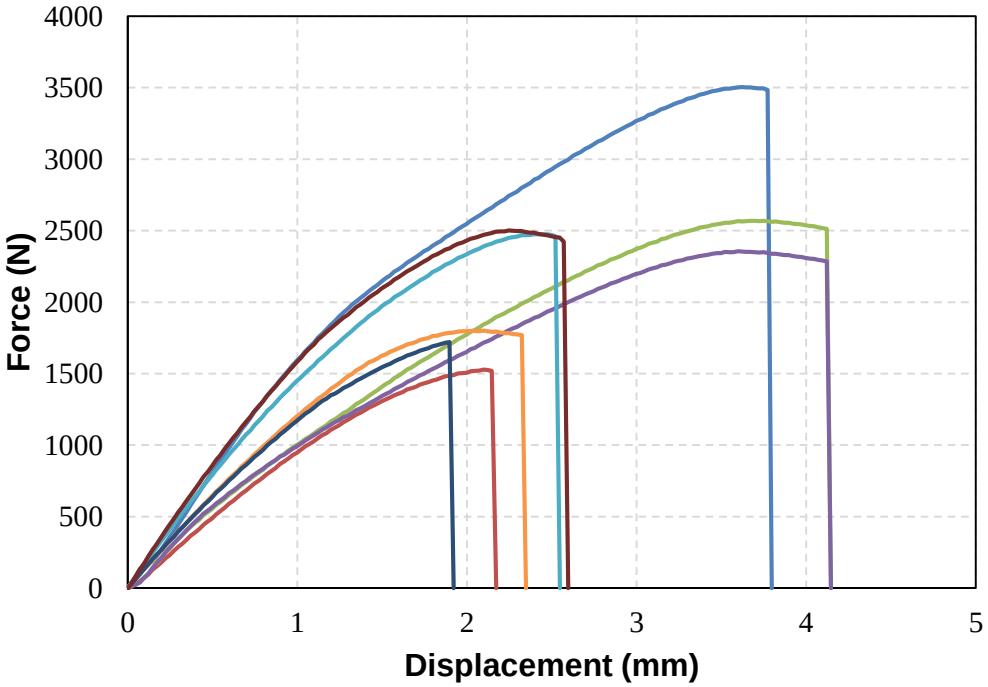

Figure 38. Experimental tensile force-displacement data for specimen type T-U1.

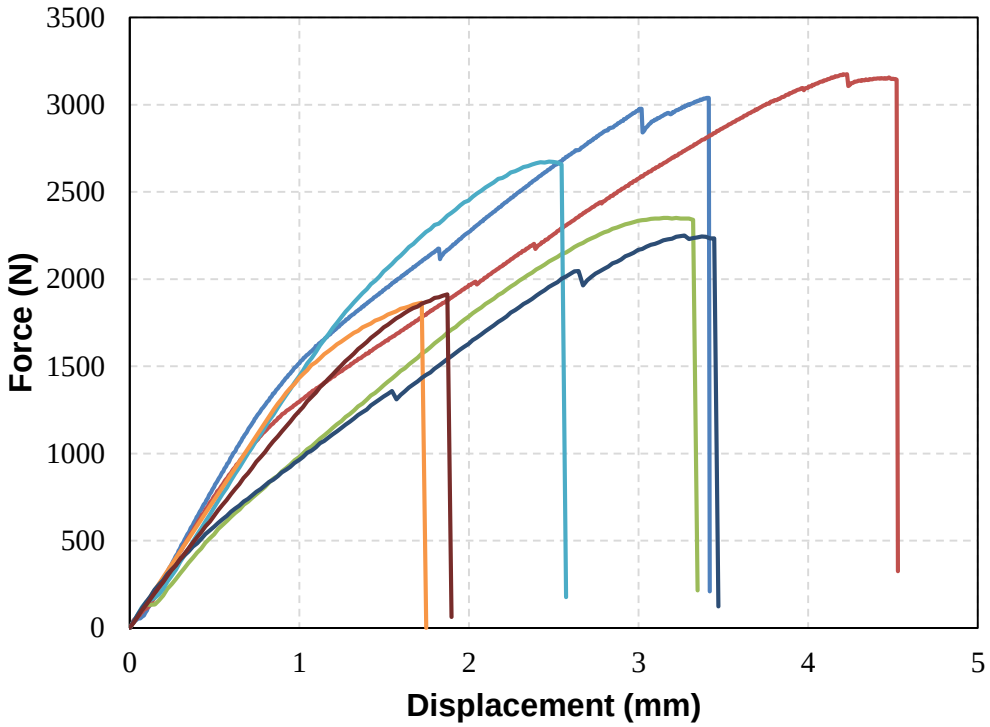

Figure 39. Experimental tensile force-displacement data for specimen type T-J1.

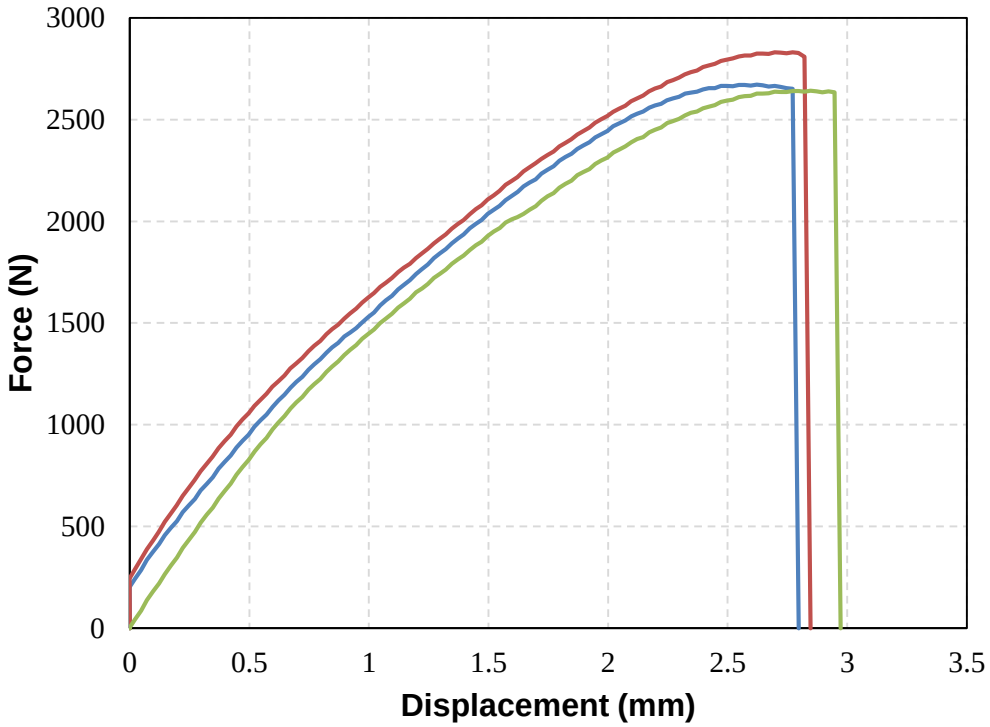

Figure 40. Experimental tensile force-displacement data for specimen type T-F1.

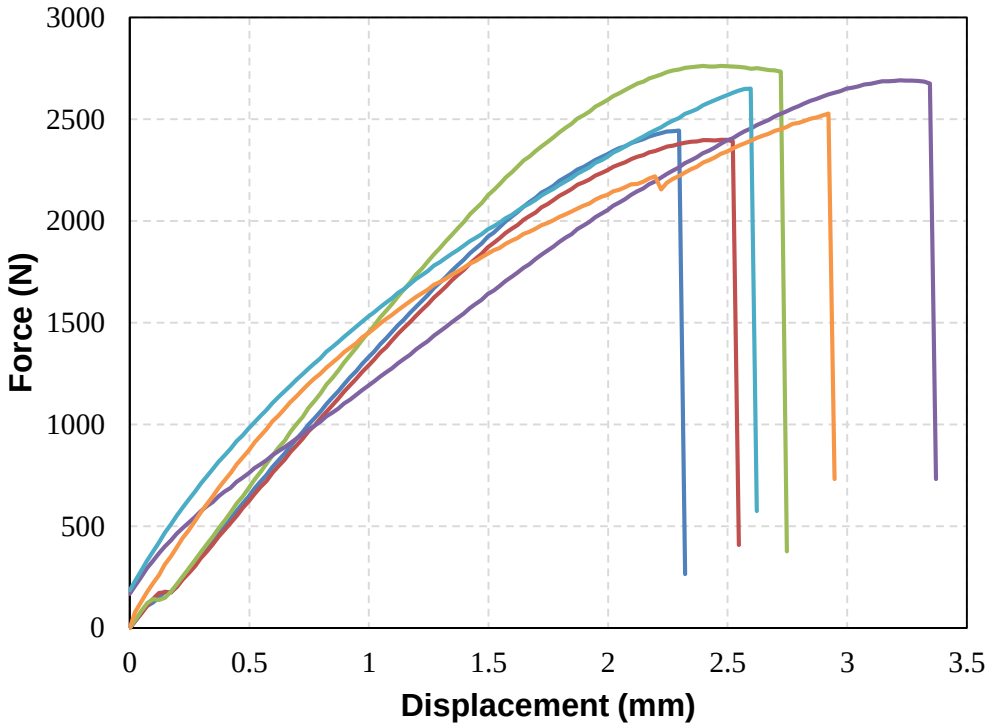

Figure 41. Experimental tensile force-displacement data for specimen type T-F2.

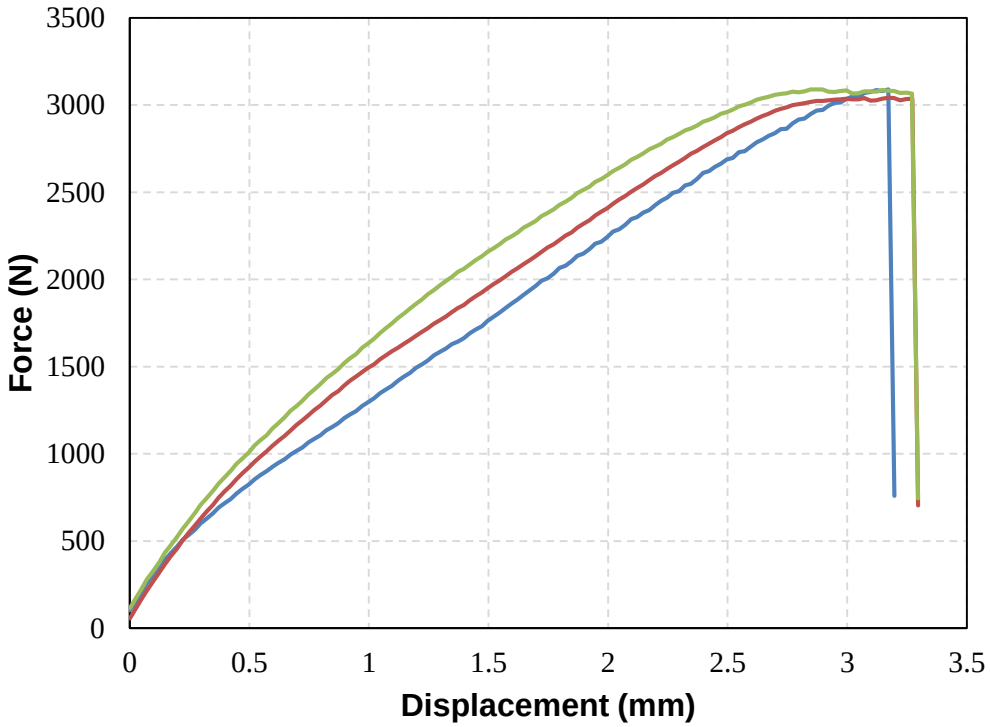

Figure 42. Experimental tensile force-displacement data for specimen type T-F3.

APPENDIX B

Flexural Data

B.1 Composite Specimen Flexural Test Data

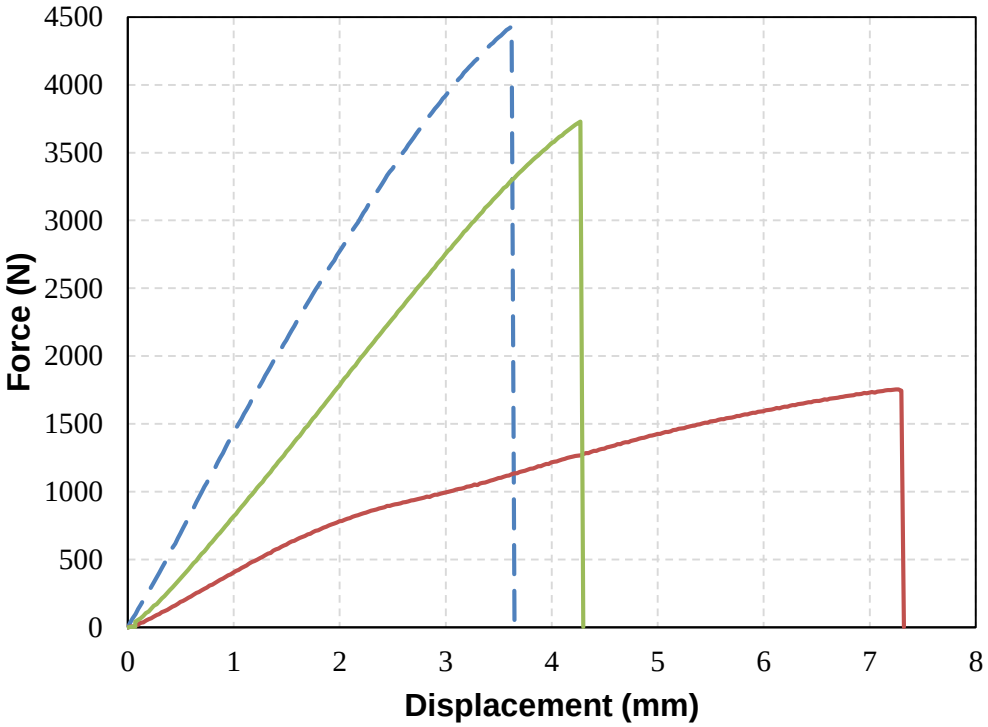

Figure 43. Experimental flexural force-displacement data for specimen type F-R-S1 of span lengths 110 mm (— —) and 135 mm (—).

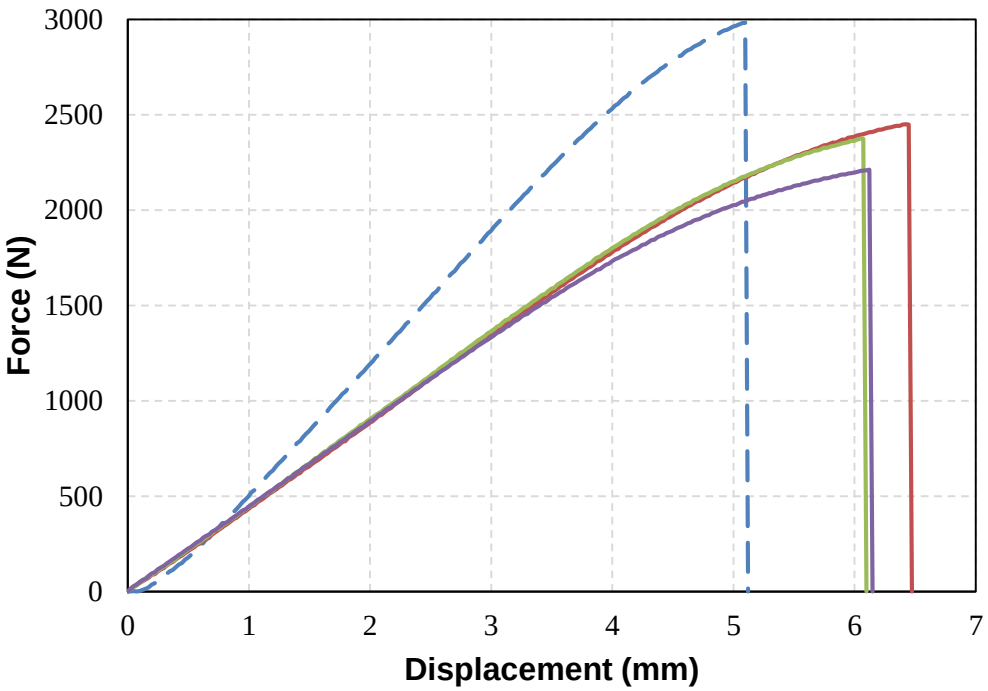

Figure 44. Experimental flexural force-displacement data for specimen type F-I-S1 of span lengths 135 mm (— —) and 160 mm (—).

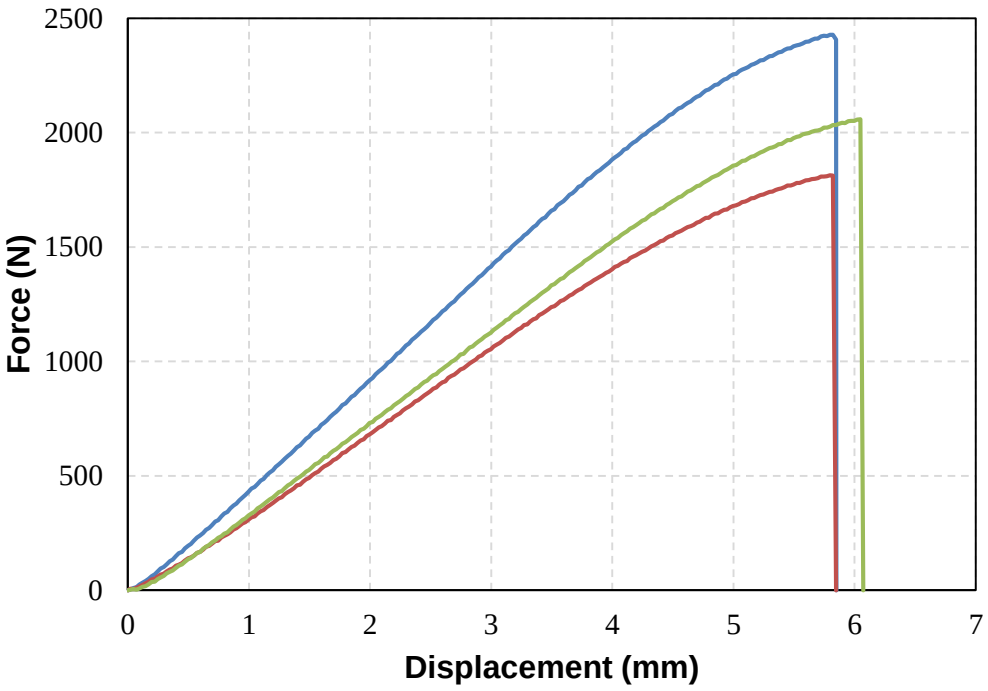

Figure 45. Experimental flexural force-displacement data for specimen type F-I-U1 of span length 160 mm.

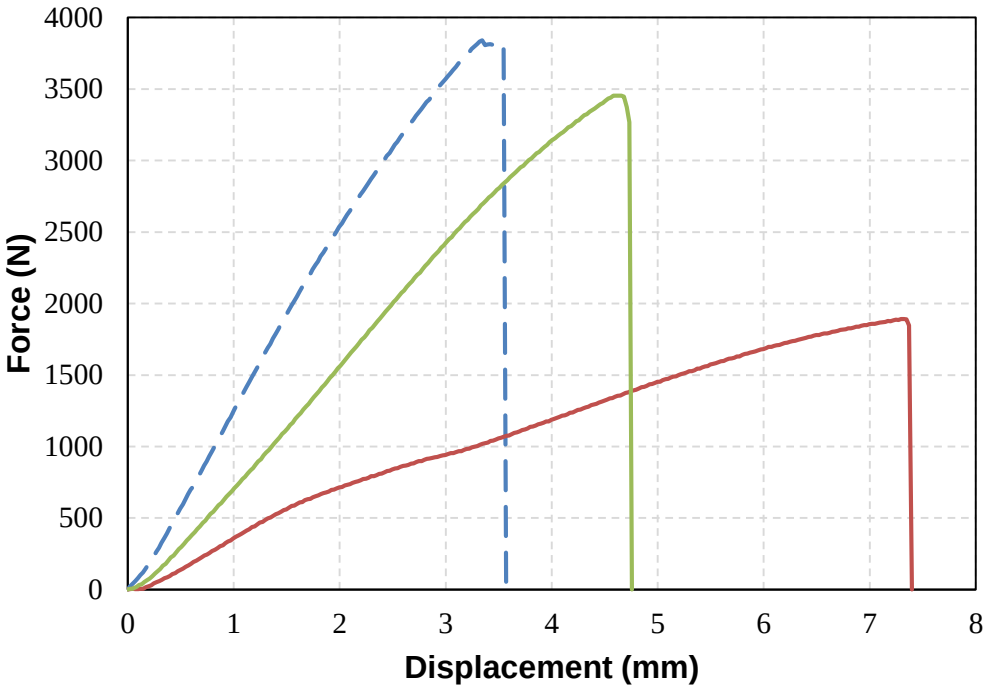

Figure 46. Experimental flexural force-displacement data for specimen type F-R-J1 of span lengths 110 mm (— —) and 135 mm (—).

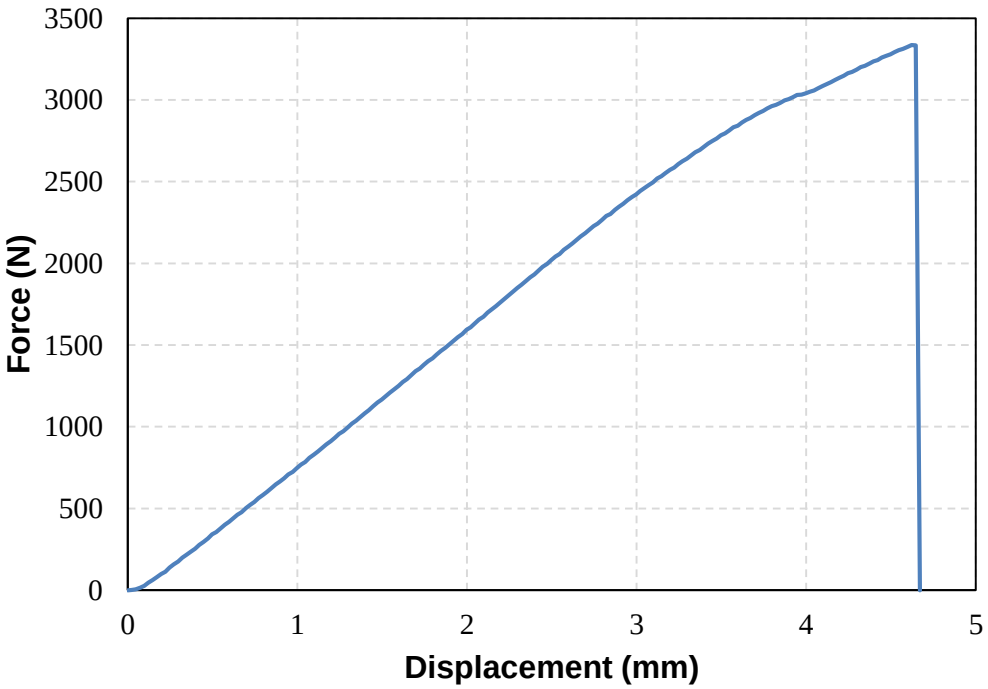

Figure 47. Experimental flexural force-displacement data for specimen type F-R-J2 of span length 135 mm.

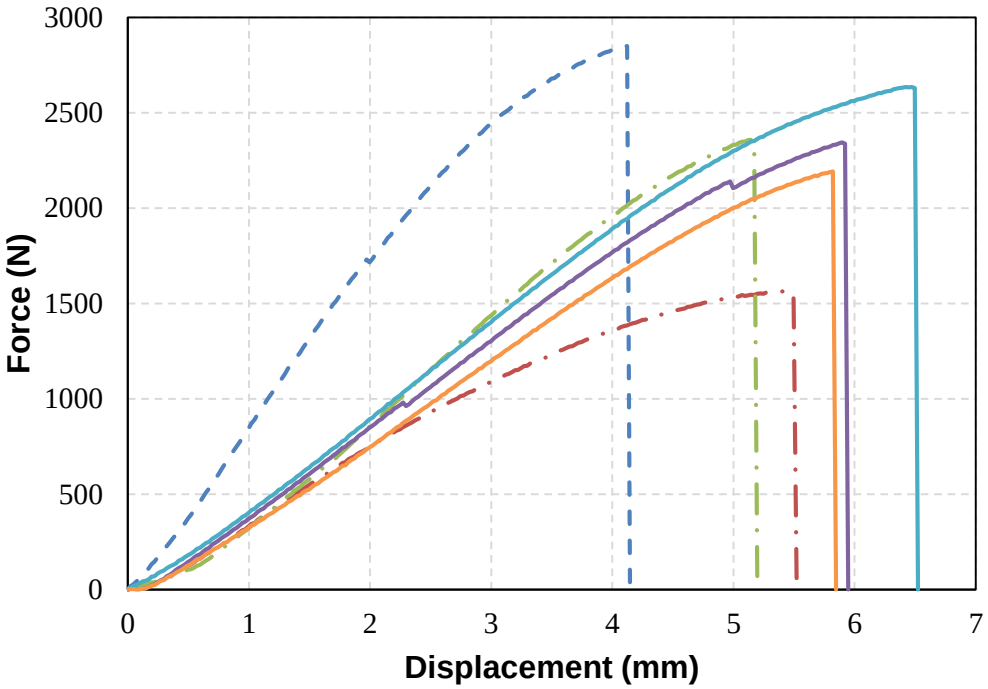

Figure 48. Experimental flexural force-displacement data for specimen type F-I-J1 of span lengths 110 mm (— —), 135 mm (— • —), and 160 mm (—).

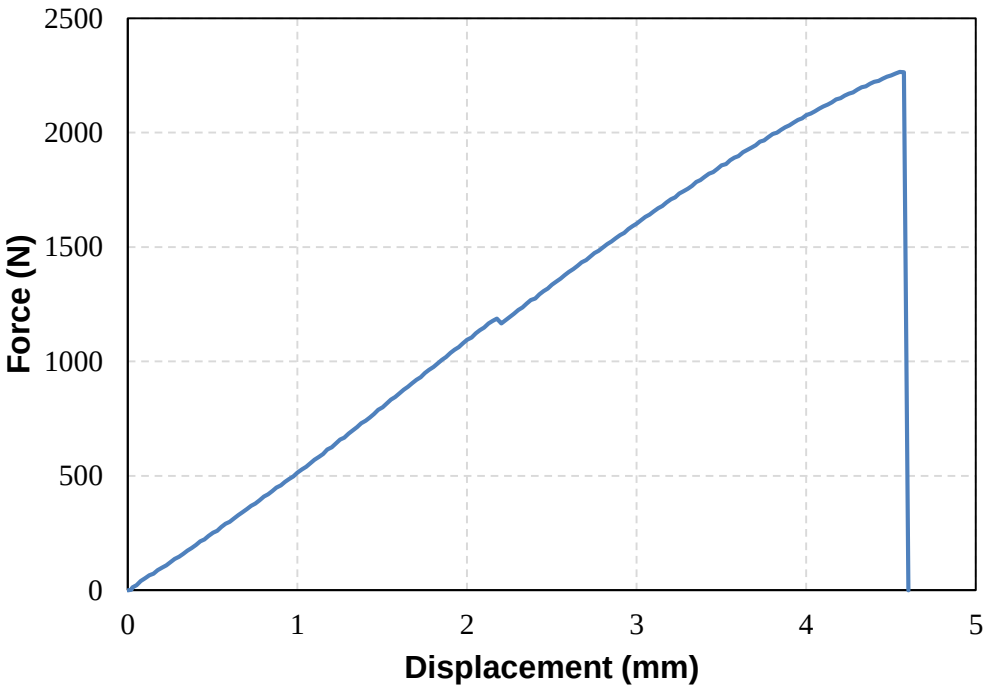

Figure 49. Experimental flexural force-displacement data for specimen type F-I-J2 of span length 135 mm.

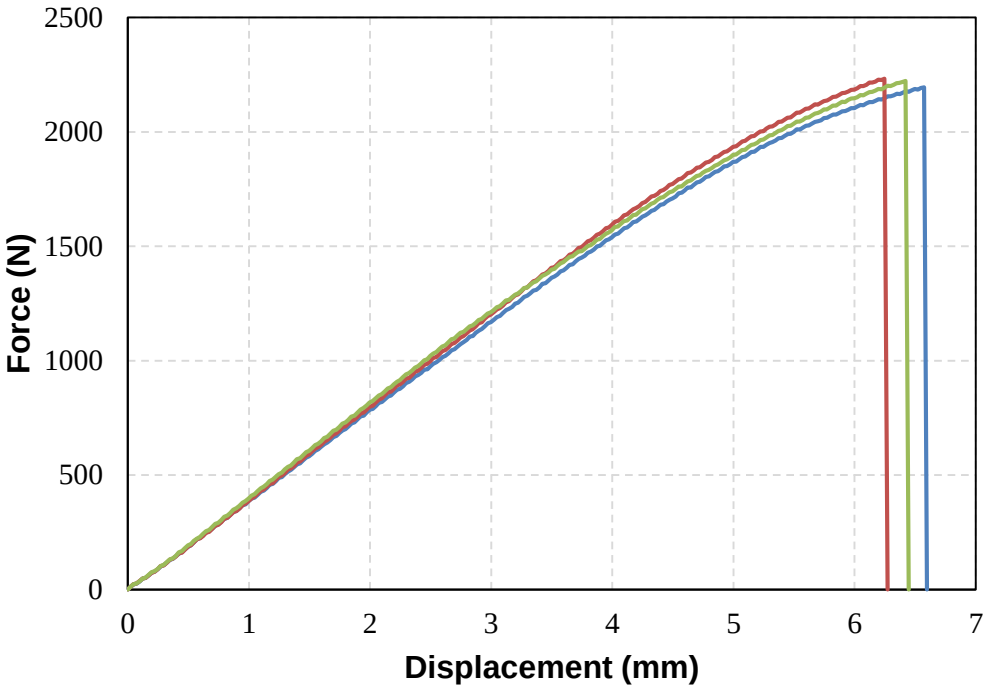

Figure 50. Experimental flexural force-displacement data for specimen type F-I-F1 of span length 160 mm.

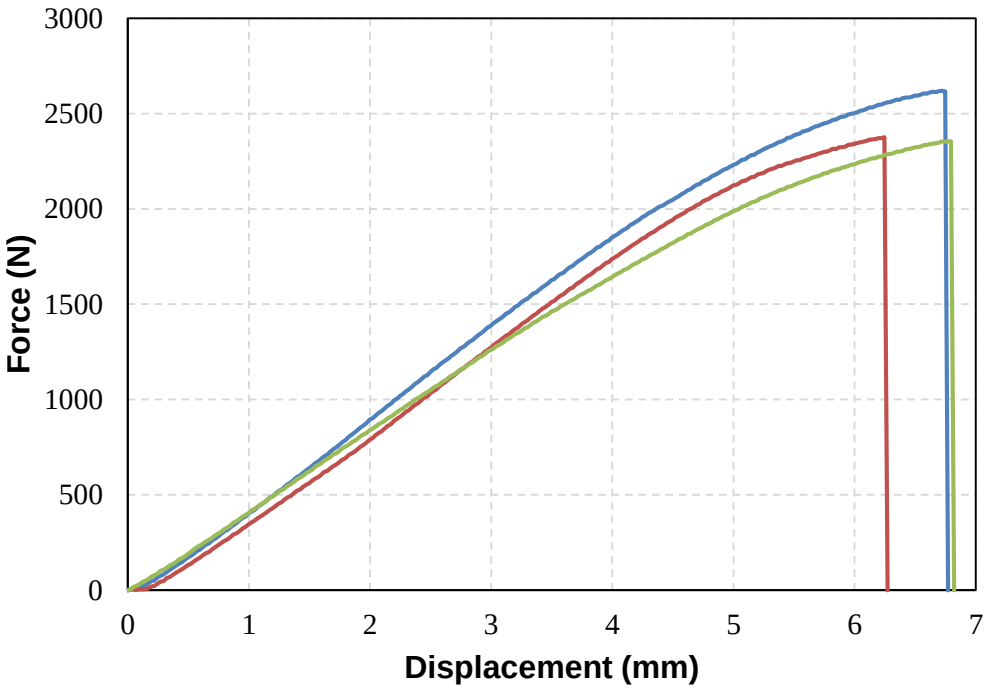

Figure 51. Experimental flexural force-displacement data for specimen type F-I-F2 of span length 160 mm.